$NASA$ $CR - 159,202$

NASA Contractor Report 159202

Investigation of the Interference Effects of Mixed-Flow Long-Duct Nacelles on a DC-10 Wing

S. P. Patel and
J. E. Donelson

Douglas Aircraft Company
McDonnell Douglas Corporation
Long Beach, CA 90846

APR 1 1979

FOR EARLY DOMESTIC DISSEMINATION

National Aeronautics and
Space Administration

Langley Research Center
Hampton, Virginia 23665
AC 804 827-3966

1. Report No. NASA CR-159202	2. Government Accession No.	3. Recipient's Catalog No.
4. Title and Subtitle Final Report — Investigation of the Interference Effects of Mixed-Flow Long-Duct Nacelles on a DC-10 Wing		5. Report Date 19 February 1980
		6. Performing Organization Code ACEE-05-FR-9845
7. Author(s) S. P. Patel and J. E. Donelson		8. Performing Organization Report No.
		10. Work Unit No.
9. Performing Organization Name and Address Douglas Aircraft Company McDonnell Douglas Corporation 3855 Lakewood Boulevard Long Beach, California 90846		11. Contract or Grant No. NAS1-14743
12. Sponsoring Agency Name and Address National Aeronautics and Space Administration Washington, D. C. 20546		13. Type of Report and Period Covered Contractor Report
		14. Sponsoring Agency Code

15. Supplementary Notes

Project TRCO, D. L. Maiden
Energy Efficient Transport Technology Project,
NASA Langley Research Center, Hampton, Virginia 23665

16. Abstract

This report presents the results of a wind-tunnel test utilizing a 4.7-percent-scale semi-span model in the Ames Research 11-foot transonic wind tunnel. The objective of the test program was to develop a low-drag long-duct nacelle installation for the DC-10 jet transport. A long-duct nacelle representative of a CF6-50 mixed-flow configuration was investigated on the DC-10-30. The results of this investigation showed that the long-duct nacelle installation located in the same position as the current short-duct nacelle and with the current production symmetrical pylon is a relatively low-risk installation for the DC-10 aircraft. Tuft observations and analytical boundary layer analysis confirmed that the flow on the nacelle afterbody was attached. A small pylon fairing was evaluated and found to reduce channel peak suction pressures, which resulted in a small drag improvement. The test also confirmed that the optimum nacelle incidence angle is the same as for the short-duct nacelle, thus the same engine mount as for the production short-duct nacelle can be used for the long-duct nacelle installation. Comparison of the inboard wing-pylon-nacelle channel pressure distributions, with flow-through and powered long-duct nacelles showed that the power effects did not change the flow mechanism; hence, power effects can be considered negligible.

17. Key Words (Suggested by Author(s)) Short-duct nacelle (SDN) Long-duct nacelle (LDN) Flow-through Powered Cruise drag reduction Channel pressure distribution	18. Distribution Statement FEDD Distribution N80-72441#
19. Security Classif. (of this report) Unclassified	20. Security Classif. (of this page) Unclassified	21. No. of Pages 66	22. Price*

*Available: NASA's Industrial Applications Centers

N-305

FOREWORD

This document presents the results of a contract study for the National Aeronautics and Space Administration (NASA) by the Douglas Aircraft Company, McDonnell Douglas Corporation. This work is part of Phase I, Energy Efficient Transport (EET) project, of the Aircraft Energy Efficient (ACEE) program. The study consisted of long-duct nacelle and pylon wind tunnel development work applied to the DC-10 to achieve a low-cruise-drag configuration.

The NASA technical monitor for the contract was Mr. D. L. Maiden of the Energy Efficient Transport Project Office at Langley Research Center. Acknowledgement for support and guidance is also given to Mr. J. R. Tulinius, the on-site NASA representative. Acknowledgement is also given to the Director and staff of the Ames Research Center at which the test program was conducted.

Douglas personnel who made significant contributions to this work are:

M. Klotzsche	ACEE Program Manager
A. B. Taylor	EET Project Manager
0. D. Wells	Aerodynamic Design, Task Manager for Test Phase
J. E. Donelson	Aerodynamic Design, Task Manager for Post-Test Phase (report coauthor)
S. P. Patel	Aerodynamic Design (report coauthor)
J. T. Callaghan	Aerodynamic Project Engineer - EET
J. D. Cadwell et al	Aerodynamics Wind Tunnel - Model Group

CONTENTS

FIGURES

FIGURES

TABLES

LIST OF SYMBOLS

All force data presented in this report have been reduced to coefficient form based on trapezoidal semispan wing area. Pressure data have been reduced to coefficient form with reference to freestream pressures. All dimensional values are given in both International Systems of Units (SI) and U.S. Customary Units, the principal measurements and calculations using the latter.

Coefficients and symbols used herein are defined as follows:

A Area, m^2 (ft^2)

b_w Reference wing span, 236.86 cm (93.25 in.)

C_D Drag coefficient, $\left(\dfrac{Drag}{q_\infty S_w}\right)$

ΔC_D Incremental drag coefficient

C_f Skin friction coefficient

C_L Lift coefficient, $\left(\dfrac{Lift}{q_\infty S_w}\right)$

C_p Pressure coefficient, $\left(\dfrac{P_\ell - P_\infty}{q_\infty}\right)$

c_w Local wing chord, cm (in.)

$\bar{c}_w$ Reference wing mean aerodynamic chord, 35.3 cm (13.9 in.)

g Acceleration due to gravity, m/S^2 (ft/sec^2)

M_{DIV} Drag divergence Mach number

M_∞ Freestream Mach number

M_L Local Mach number

P_T Total pressure, N/m^2 (lb/ft^2)

P_{T_F} Fan exit total pressure, N/m^2 (lb/ft^2)

P_ℓ Local static pressure, N/m^2 (lb/ft^2)

P_∞ Freestream static pressure, N/m^2 (lb/ft^2)

q_∞ Freestream dynamic pressure, N/m^2 (lb/ft^2)

R Reynolds number per meter (per foot)

S_W Reference semispan wing area, 0.3743 m^2 (4.029 ft^2)

X Spanwise distance from fuselage centerline, cm (in.)

Y Distance along fuselage centerline, cm (in.)

Z_{WN} Vertical coordinates from nacelle centerline, cm (in.)

θ_{NAC} Nacelle incidence angle, degrees

α_F Fuselage angle of attack, degrees

ACRONYMS

ACEE	Aircraft Energy Efficiency (Program)
ARC	Ames Research Center
EET	Energy Efficient Transport (Project)
GE	General Electric Company
LDN	Long-duct nacelle
NPR	Nozzle pressure ratio
RPM	Revolutions per minute
SDN	Short-duct nacelle
SFC	Specific fuel consumption

SUMMARY

This report presents the results of a wind tunnel test, the objective of
which was to develop a low-drag long-duct nacelle installation for the DC-10
jet transport. The study was conducted as part of the NASA Energy Efficient
Transport (EET) program. A long-duct nacelle representative of a General
Electric (GE) CF6-50 mixed-flow configuration installed on the wing position
of the DC-10-30 jet transport, was investigated. The investigation was
conducted in the NASA Ames Research Center 11-foot transonic wind tunnel
using a 4.7-percent-scale semispan model of the DC-10-30. The test was
carried out over a Mach number range of 0.6 to 0.84 and over a lift coeffi-
cient range up to 0.60 at a constant Reynolds number of 18.0×10^6 per meter
$(5.5 \times 10^6$ per foot).

The results of this investigation showed that the long-duct nacelle installa-
tion located in the same position as the current short-duct nacelle and with
the current production symmetrical pylon is a relatively low-risk installation
for the DC-10 aircraft. Tuft observations and analytical boundary layer
analyses confirmed that the flow on the nacelle afterbody was attached. A
small pylon fairing was evaluated and found to reduce channel peak suction
pressures which resulted in a small drag improvement. The test also con-
firmed that the optimum nacelle incidence angle is the same as for the short-
duct nacelle, thus the same engine mounts used for the production short-duct
nacelle can be used for the long-duct nacelle installation. Comparison of
the inboard wing-pylon-nacelle channel pressure distributions, with flow-
through and powered long-duct nacelles, showed that the power effects did
not change the flow mechanism. Therefore, power effects can be considered
negligible.

INTRODUCTION

At the beginning of the Energy Efficient Transport (EET) project, one concept selected for development towards potential application on DC-10 aircraft derivatives was the mixed-flow long-duct nacelle.

Early in 1974, a study was started by Douglas and continued under NASA contract to examine the potential improvements obtainable by using a mixed-flow long-duct nacelle (LDN) on the DC-10. The study (Reference 1) showed that in addition to potential noise reductions, a mixed-flow long-duct nacelle incorporating advanced composites structure offered a significant improvement in specific fuel consumption (SFC). The gains arose from (1) the improvement in propulsive efficiency due to the internal mixing of the fan and primary streams which, for the separate flow nacelle, exit at different velocities, and (2) from the elimination of the nacelle afterbody jet scrubbing drag. On the debit side, the freestream scrubbing drag was increased due to the longer fan cowl. In addition, it was estimated that a further improvement would result from the reduction of the wing-pylon-nacelle channel velocities that result from the influence of the wing pressure flow field on the nacelle cyclic flow field. It was estimated that a total of 4- to 5-percent improvement in fuel burned could be realized by the application of the LDN installation.

However, care must be exercised to prevent access wing-pylon-nacelle interference drag from diluting this potential gain. History relates that both the Convair 990 (Reference 2) and the Douglas DC-8 prototype LDN installations suffered severe nacelle interference drag penalties prior to aerodynamic modifications. These deficiencies were characterized by high velocities in the channel bounded by the inboard side of the nacelle, pylon, and wing lower surface resulting in shock waves of sufficient strength to cause flow separations on the nacelle and pylon. The shock waves resulted from the superposition of the nacelle, pylon, and wing peak velocities resulting in much higher velocities than for the isolated components. The classic approaches to minimize this phenomenon are (1) to offset the interfering pressure peaks and (2) cambering the pylon geometry to reduce the channel peak suction pressures. The DC-10 uses nearly common aerodynamic lines for

1

all of the wing engine installations so it is desirable to retain the existing pylon, if possible; i.e., keep the nacelle located in the same position as for the current short-duct nacelle (SDN). This constraint also is desirable from the standpoint of using the existing engine mount arrangement. It has been shown that for the high bypass fan engines, it is important to achieve the optimum nacelle incidence because the nacelle can incur fairly significant induced drag penalties if allowed to carry much lift. This is the reason for the small nacelle incidence angle on the DC-10. It was necessary, therefore, to determine if any change to the nacelle incidence (i.e., engine mounts) was required with the nacelle fan cowl extended further aft under the wing.

The purpose of this investigation was to develop a low-drag LDN installation for the DC-10. Work was accomplished by a development program conducted in the NASA Ames Research Center 11-foot transonic wind tunnel (hereafter referred to as the ARC 11-foot wind tunnel) in June-July 1978. The configurations for the program were designed by using the Douglas Neumann potential flow computer code (Reference 3). The Gothert compressibility corrections are incorporated in the calculations.

The model used for this investigation was a 4.7-percent scale semispan model of a DC-10-30 aircraft. Nacelle simulation was by flow-through nacelle and by turbo-simulator using the Tech Development TD-460 4.1-inch simulator. The latter was used to examine the effects of power. The LDN aerodynamic lines were developed under NASA Contract NAS1-13356 (Reference 1) and represent those for the installation of a General Electric (GE) CF6-50 high bypass fan engine.

All configurations had the LDN located in the same location as for the current production SDN installation. The baseline configuration used the SDN production symmetrical pylon.

Two pylon fairings designed to reduce local velocities in the inboard wing-pylon-nacelle channel were evaluated with the flow-through LDN.

2

The effects of increased and decreased LDN incidence angle were assessed relative to the nacelle incidence of the production SDN installation.

Aerodynamic forces as well as wing, pylon, and nacelle surface pressure data were measured during the test. Tufts were installed on the LDN afterbody and pylon near the nacelle juncture to observe flow quality in the channel.

NACELLE-PYLON CONFIGURATION DESIGN
## Long-Duct Nacelle Design

The nacelle (Figure 1) was designed according to the recommendations reported in Reference 1 except that the inlet was modified to preclude excess spillage drag for the model. For a flow-through nacelle, freestream flow entering the inlet is controlled by the nacelle exit area. If the afterbody is accurately represented, this will result in less mass flow through the inlet than for the full-scale engine nacelle due to the fact that no work is being done on the simulator mass flow (i.e., exit momentum approximately equal to entering momentum). This creates a low inlet mass flow ratio for the flow-through nacelle resulting in premature spillage drag and a lower drag-divergence Mach number for the inlet cowl. The inlet cowl was modified by decreasing the cowl diameter ratio (leading to maximum diameter ratio) to achieve the same drag divergence as for the full-scale CF6 inlet cowl (i.e., N_{DIV} = 0.85).

The current production DC-10 symmetrical pylon was selected as the baseline configuration, resulting in the retention of the SDN incidence of 0.9 degree nose up. Incidence angle variations of ±1.5 degrees from the baseline were incorporated into the pylon geometry in order to evaluate the minimum-drag incidence angle for the LDN. The current toe-in angle of 2.0 degrees was retained for the LDN configurations.

Pylon Fairing Design

A simplified-panel potential flow model of the wing plus LDN and pylon was developed and used to evaluate a number of pylon configurations with systematic variations in shape. The study examined the effects of pylon leading and training edge camber and selected pylon fairings on the wing-pylon-nacelle channel pressure distributions. The simplified model was used only to indicate trends and to guide the design selection process. Selected configurations were subsequently evaluated with a more comprehensive fine-panel model.

A. CF6-50 MIXED-FLOW LDN
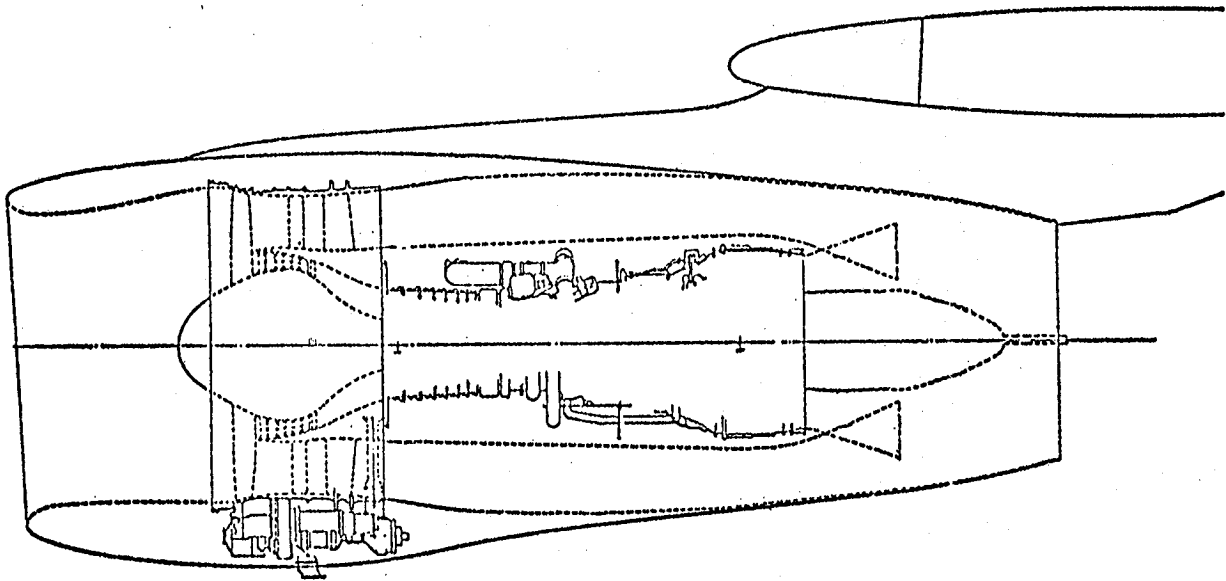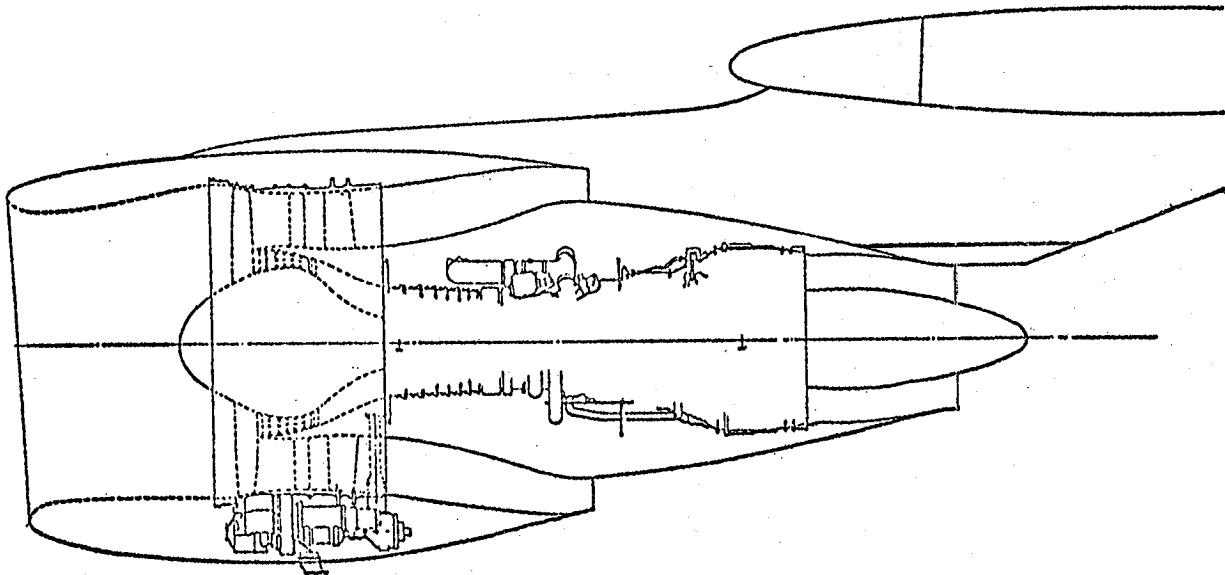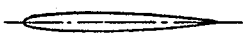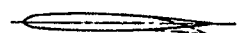

B. CF6-50 PRODUCTION SDN
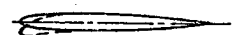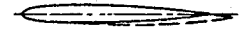
FIGURE 1. CF6-50 PRODUCTION SDN AND MIXED-FLOW LDN

The pylon modifications considered during the design selection process and summary of the results of the analysis are shown in Table 1.

The largest predicted benefit was offered by Configurations E and G. Configuration E employed a small aft fairing and Configuration G combined this fairing with large leading-edge fairing. These configurations were then investigated using the more detailed method. The previous estimates for Configuration G were found to be optimistic relative to the fine-panel results and it was therefore discarded. Configuration E revisions were required to retain its performance and the resulting shape was denoted as Configuration J. In order to effect a further reduction in the channel suction peaks, a modification of the J-type fairing incorporating a larger aft fairing was defined, and this was designated Configuration K. Configurations J and K were selected for the experimental work. In each case, the pylon fairings were designed to be external to the DC-10 pylons so that the primary structure and systems routing would be unaffected. The pylon wetted area as well as the pylon overhang was increased with both the smaller and the larger pylon fairings.

The calculated potential flow pressure distributions on the wing lower surface, pylon, and nacelle in the vicinity of the inboard channel for the baseline symmetrical pylon, the small (Configuration J) and the large (Configuration K) pylon fairings, using the detailed fine-panel potential flow model, are presented in Figure 2. The fairings reduce the levels of the suction peaks near the channel throat and increase the suction levels 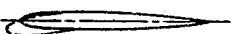aft of the throat, simultaneously tending to reduce the throat Mach number and the severity of the diffusion pressure gradient aft of the throat. This is evident all across the channel.

TABLE 1
SUMMARY OF PYLON DESIGN ANALYSIS
(RIGHT PYLON SHOWN)

USING SIMPLIFIED NEUMANN PANEL GRID

CONFIGURATION	TYPE OF FAIRING	REDUCTION IN WING LOWER SURFACE $C_{P_{PEAK}}$	WING LOWER SURFACE AND PYLON PRESSURE GRADIENT AFT OF $C_{P_{PEAK}}$	REMARK
	SYMMETRICAL PYLON	—	BASE	SYMMETRICAL PYLON IS USED AS THE BASELINE CONFIGURATION
A	SMALL AFT CAMBER	+0.01	WORSE	GRADIENT AFT OF PEAK PRESURE IS MORE SEVERE ON WING LOWER SURFACE AND PYLON
B	LARGE AFT CAMBER	+0.04	WORSE	GRADIENT ON WING LOWER SURFACE AND PYLON IS MORE SEVERE AND WORSE THAN THAT WITH CONFIGURATION A
C	SMALL LEADING EDGE CAMBER	+0.02	SAME	NO CHANGE IN ADVERSE PRESSURE GRADIENT ON WING LOWER SURFACE AND PYLON
D	LARGE LEADING EDGE CAMBER	+0.06	SAME	NO CHANGE IN ADVERSE PRESSURE GRADIENT ON WING LOWER SURFACE AND PYLON
E	SMALL AFT FAIRING	+0.06	BETTER	LARGE REDUCTION IN PEAK PRESSURES AND ADVERSE PRESSURE GRADIENT ON WING LOWER SURFACE & PYLON
F	LARGE LEADING EDGE FAIRING	+0.09	BETTER	LARGE REDUCTION IN PEAK PRESSURES & LITTLE REDUCTION IN ADVERSE PRESSURE GRADIENT ON WING LOWER SURFACE AND PYLON
G	LARGE LEADING EDGE & SMALL AFT FAIRING E + F CONFIGURATION	+0.10	BETTER	LARGE REDUCTION IN SUCTION PEAK PRESSURES AND ADVERSE PRESSURE GRADIENT. REDUCTION IN PEAK PRESSURES FOR CONFIGURATIONS E AND F ARE NOT ADDITIVE.

USING FINE NEUMANN PANEL GRID (SELECTED FOR AMES TEST)

| CONFIGURATION	TYPE OF FAIRING	REDUCTION IN $C_{P_{PEAK}}$ WING	PYLON	NACELLE	PRESSURE GRADIENT AFT OF $C_{P_{PEAK}}$ ON WING, PYLON & NACELLE	REMARK
J	SMALL AFT FAIRING SIMILAR TO 'E'	+0.07	+0.12	+0.08	BETTER	LARGE REDUCTION IN PEAK PRESSURES AND ADVERSE PRESSURE GRADIENT ON WING, PYLON, AND NACELLE
K	LARGE AFT FAIRING LARGER THAN 'J'	+0.10	+0.14	+0.15	MUCH BETTER	SUBSTANTIAL REDUCTION IN PEAK PRESSURES AND ADVERSE PRESSURE GRADIENT ON WING, PYLON, & NACELLE
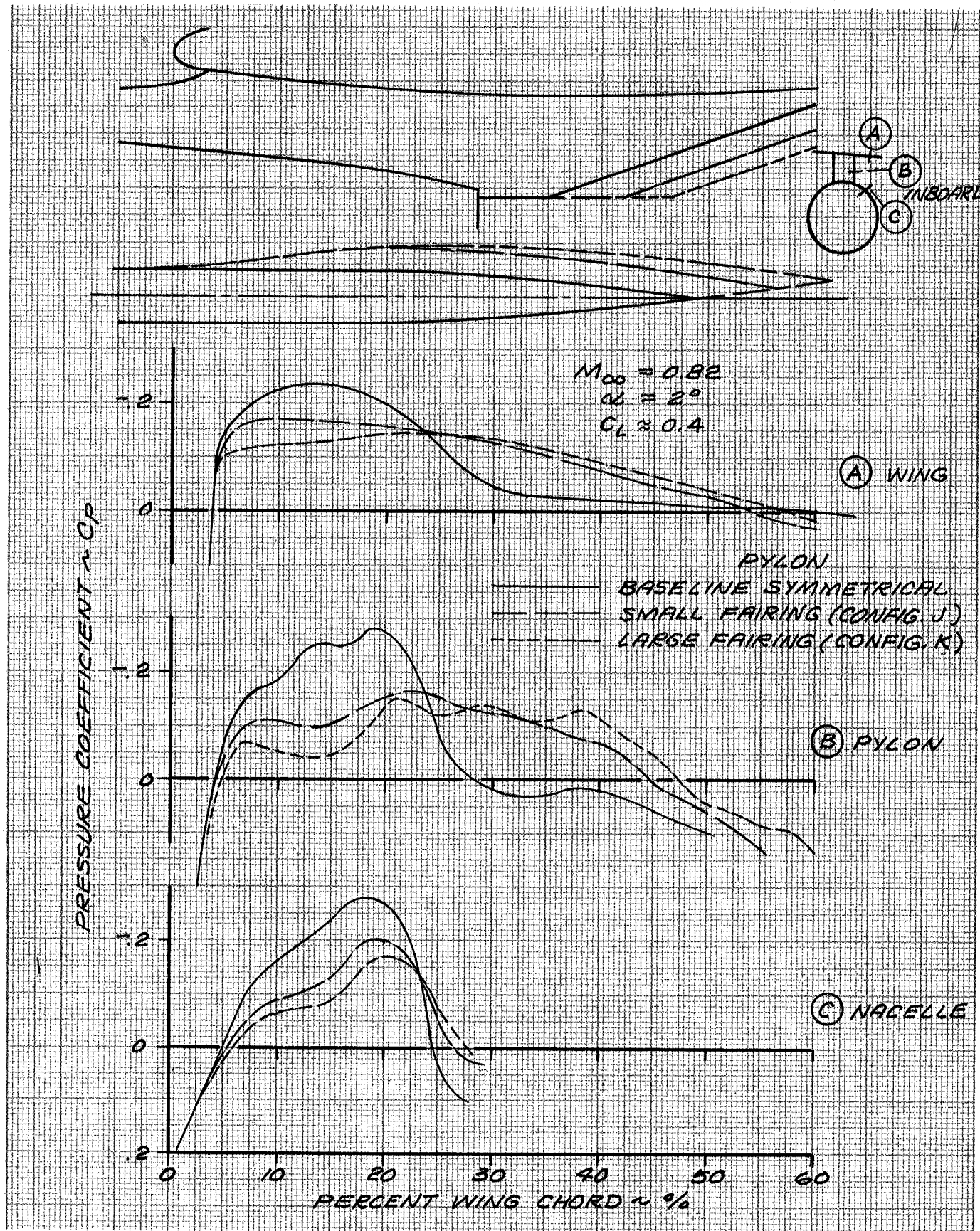
FIGURE 2. EFFECT OF PYLON FAIRINGS ON COMPUTED INBOARD CHANNEL PRESSURES

9

EXPERIMENTAL APPARATUS AND PROCEDURE
Test Facility

The test was conducted in the ARC 11-foot wind tunnel. The test section is
3.35 m (11.0 feet) square and 6.71 m (22.0 feet) long and is slotted in all
walls to provide control of the shock-wave reflection. The Mach number can
be continuously varied through the range of 0 to 1.4. A more detailed
description of this facility is found in Reference 4.

Model Installation and Description

Isolated Nacelle Calibration Model - The calibration model was comprised of
strut, nacelle, and pylon components. The isolated nacelle model was
mounted on the upper end of a 0.55-m (1.8-foot)-span metric strut (Figure 3)
which was mounted on the NASA Langley 804S-B balance using a Douglas adapter.
The strut had a NACA 0008-64 airfoil shape and was swept 45 degrees. The
balance was mounted to the Ames 11-foot tunnel balance tub with a Douglas-
furnished balance turntable adapter. Both flow-through LDN and turbo
simulator LDN and SDN were tested during the calibration.

The turbo simulator was driven by clean, dry, high-pressure air at mass-flow
rates of up to 1.23 kg/s (2.7 pounds mass per second) at pressures up to
4.65×10^6 N/m^2 (675 psia). The drive air temperature was kept at least 348K
(not higher than 358K) to prevent ice from forming on the engine simulator
parts.

All wires and pressure tubes were routed to the model aft of the balance as
shown in Figure 3. A photograph of the isolated long-duct nacelle installa-
tion in the Ames 11-foot wind tunnel is shown in Figure 4.

Semispan Model - The semispan model represented the right-hand half of the
DC-10-30 aircraft, except that the tail surfaces were removed. The model was
mounted on the NASA Langley 804S-B balance using a Douglas adapter. The
balance was mounted to the Ames tunnel balance tub with a Douglas-furnished
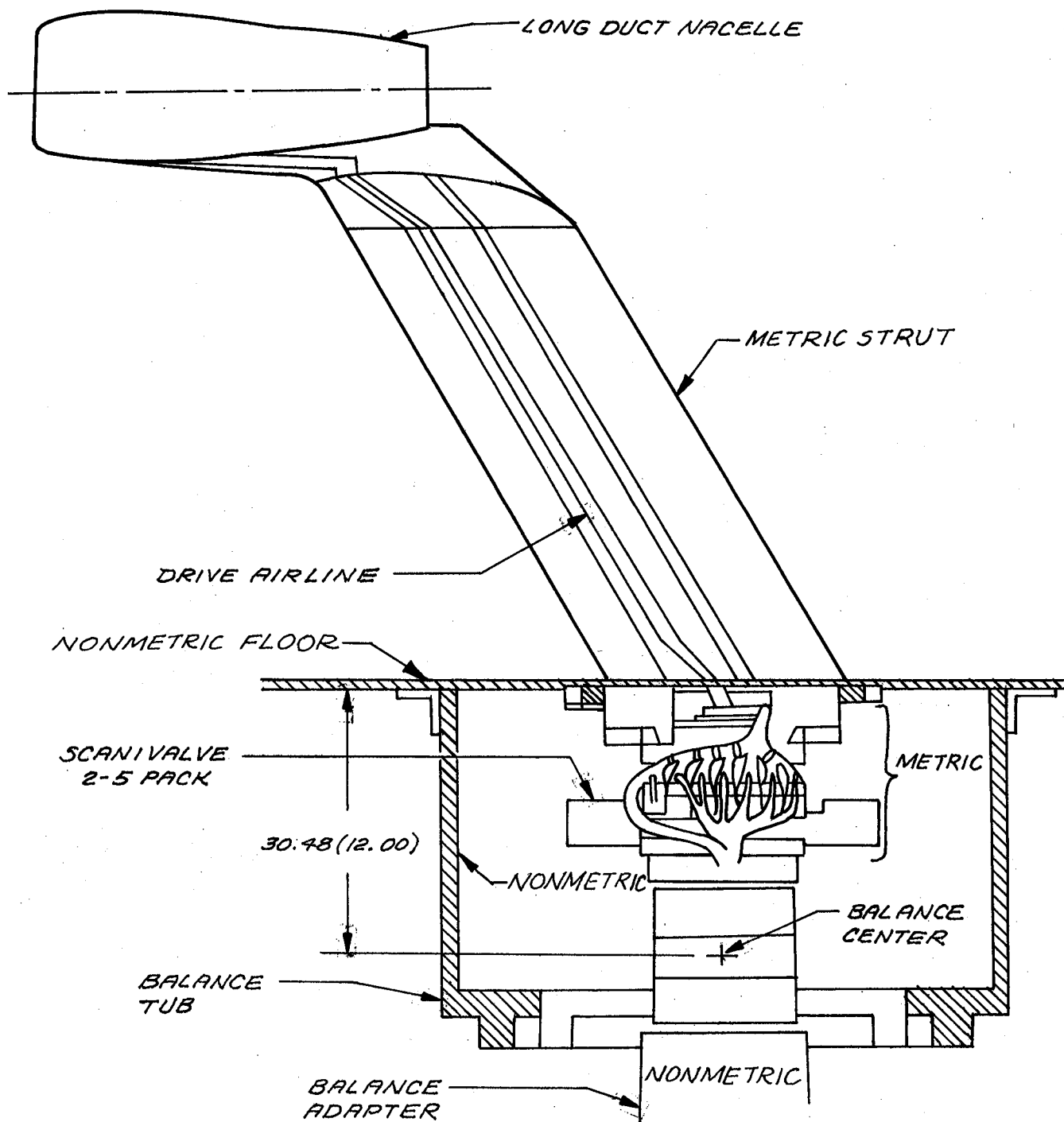balance turntable adapter.

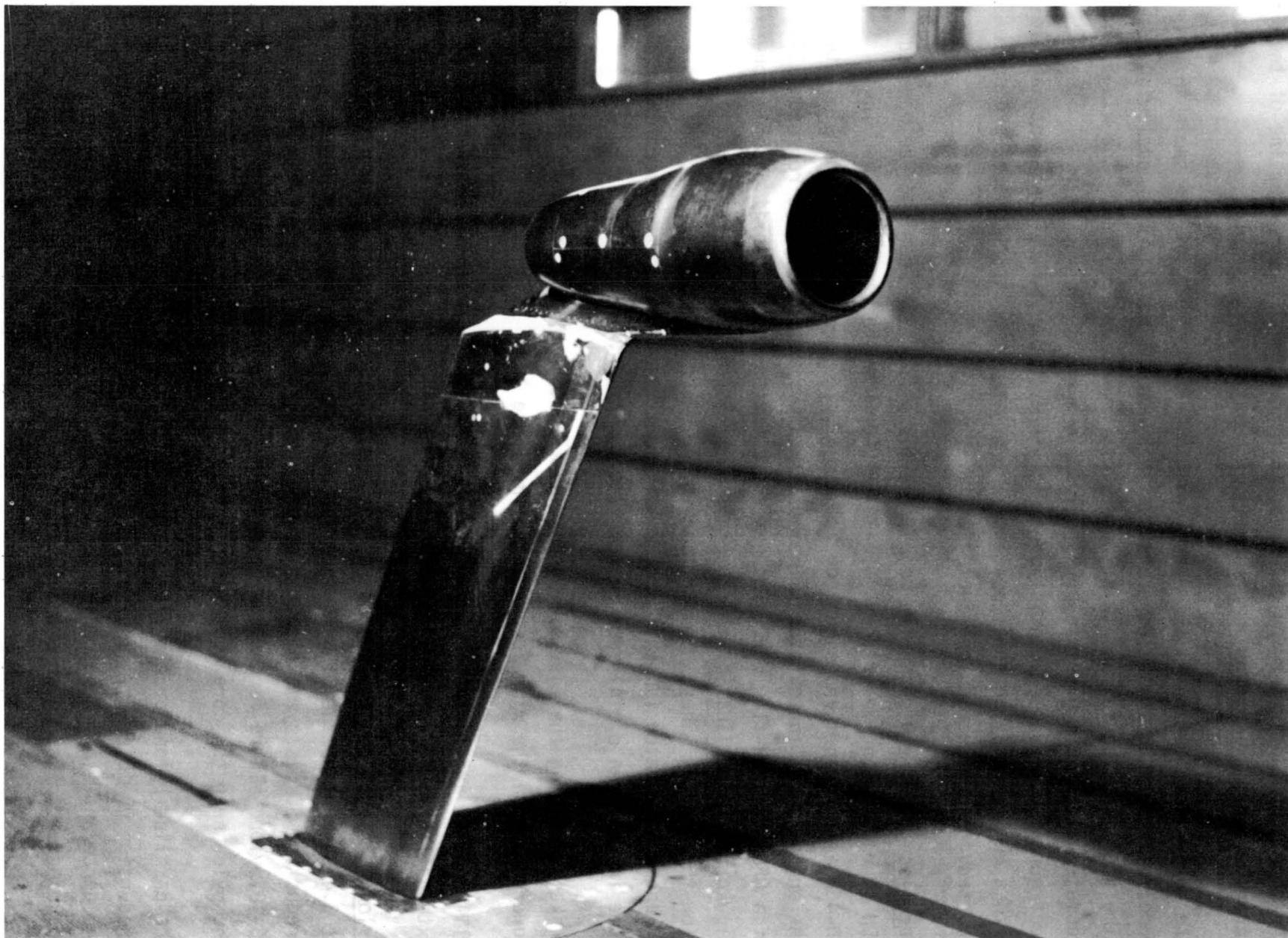FIGURE 3. ISOLATED NACELLE MODEL INSTALLATION IN AMES 11-FOOT WIND TUNNEL

FIGURE 4. PHOTOGRAPH OF ISOLATED NACELLE MODEL INSTALLATION IN AMES 11-FOOT WIND TUNNEL

The model fuselage reference plane was coincident with the centerline of the tunnel floor.

The model installation is shown in Figure 5. Photographs of the semispan model with the LDN installed are shown in Figures 6 and 7. The model wing simulated the dihedral and twist representative of 1-g loading. The wing geometry and static pressure orifice locations are shown in Figure 8. The configuration variables consist of a flow-through mixed-flow long-duct nacelle with a number of pylon configurations and a turbo simulator-powered production short-duct nacelle and long-duct nacelle.

Nacelles - Figure 9 shows the geometries of the nacelle models. The powered SDN is representative of the DC-10-30/GE CF6-50 production nacelle. The TD-460 air-driven turbo simulator is used in the powered nacelle to simulate the engine jet. The external lines of the flow-through LDN are representative of a CF6-50 mixed-flow LDN. The powered LDN is a coplanar-exit nacelle configuration. The lines of the powered LDN are nominally the same as the flow-through LDN lines; however, some minor changes were necessary because of engine simulator fan exit area requirements. The lines are essentially the same in the area of interest adjacent to the pylon.

A sketch showing the installation of the flow-through and powered LDN and the powered SDN on the wing is presented in Figure 10.

All nacelles are instrumented with one row of static orifices on the inboard external surface, as shown in Figure 11.

Pylons - All pylons are cutback pylons and intersect the wing lower surface at 3.4 percent of the wing chord. The baseline pylon for the powered production SDN is symmetrical in shape and is representative of the production DC-10 pylon. There is one row of pressure orifices on the inboard side of the pylon near the core cowl intersection, as shown in Figure 11.

The baseline pylon for the flow-through LDN is an adaptation of the current production DC-10 pylon. The pylon could be rotated vertically to vary the incidence angle of the nacelle ±1.5 degrees from the nominal setting of +0.9 degree. The 2-degree toe-in angle was retained.

$Y = 165.064$
(64.986)

$c/4$ MAC
$X = 47.503 (18.702)$
$Y = 165.448 (65.137)$

$Y = 0$

0.51 (0.20)

30.988 (12.200)

ANGLE OF ATTACK
SYSTEM ACTUATOR

DRIVE AIR LINE

BALANCE
CENTER

INSTRUMENTATION WIRE
BUNDLE
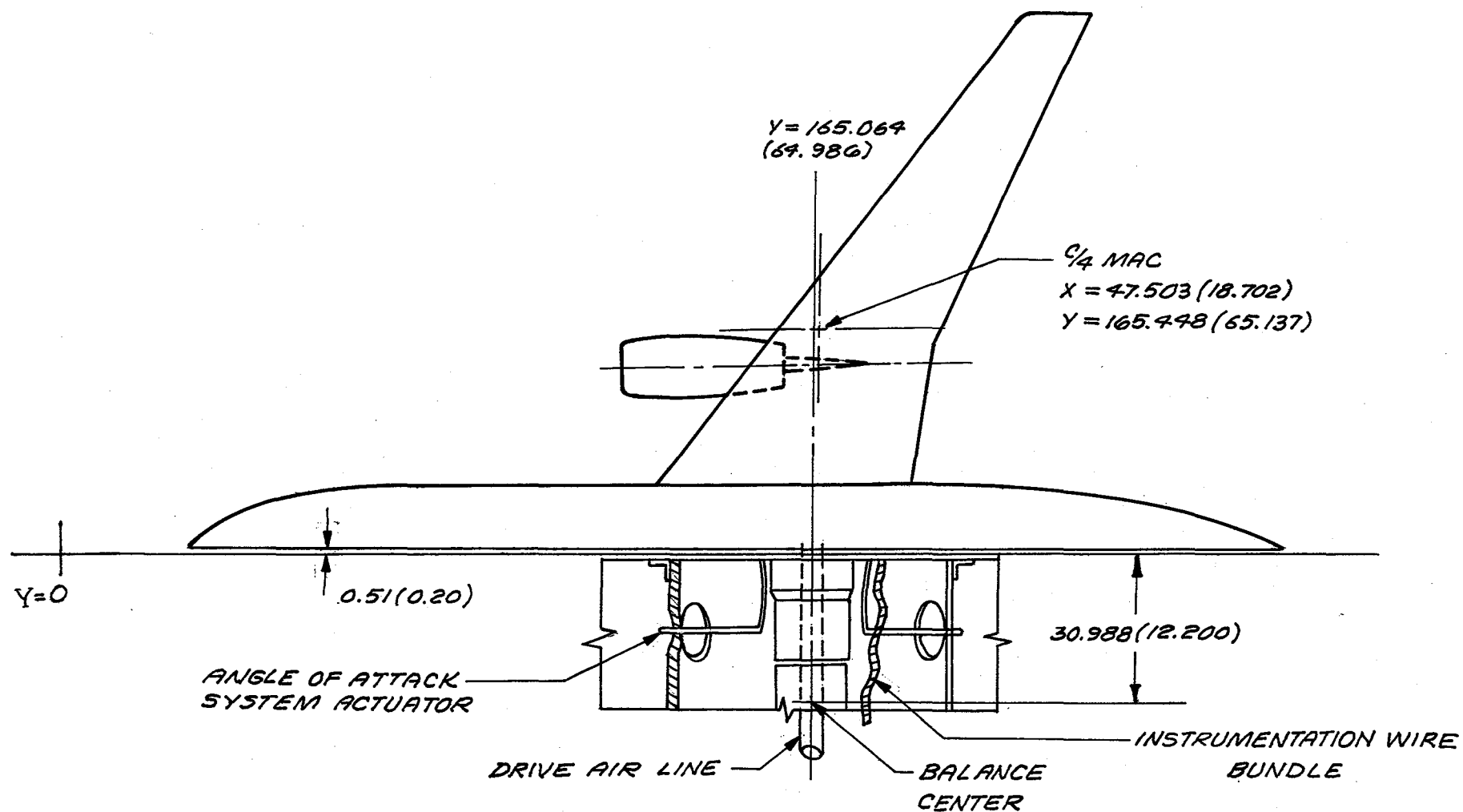
FIGURE 5. SEMISPAN MODEL INSTALLATION IN AMES 11-FOOT WIND TUNNEL
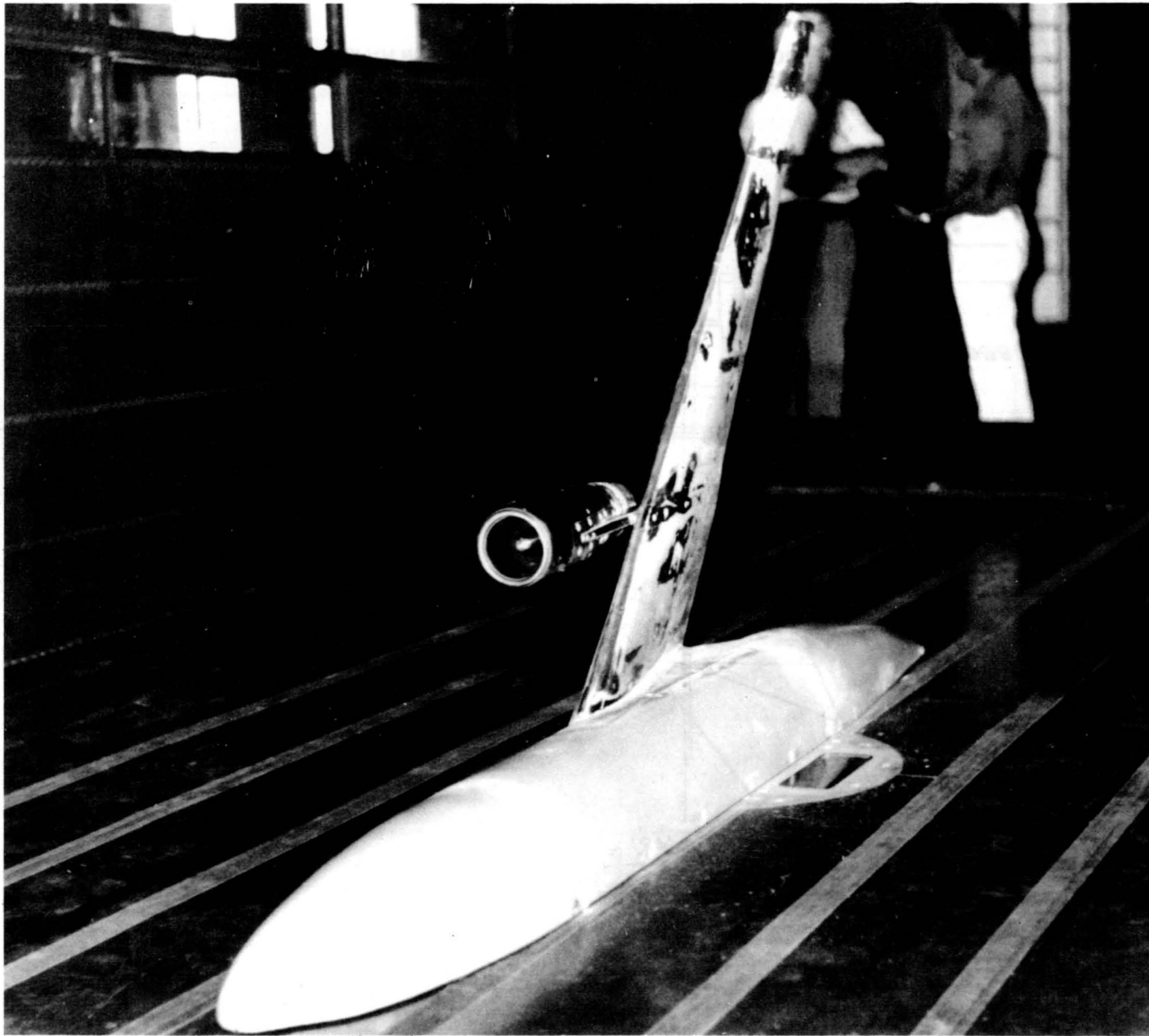
FIGURE 6. PHOTOGRAPH OF SEMISPAN MODEL INSTALLATION IN AMES 11-FOOT WIND TUNNEL
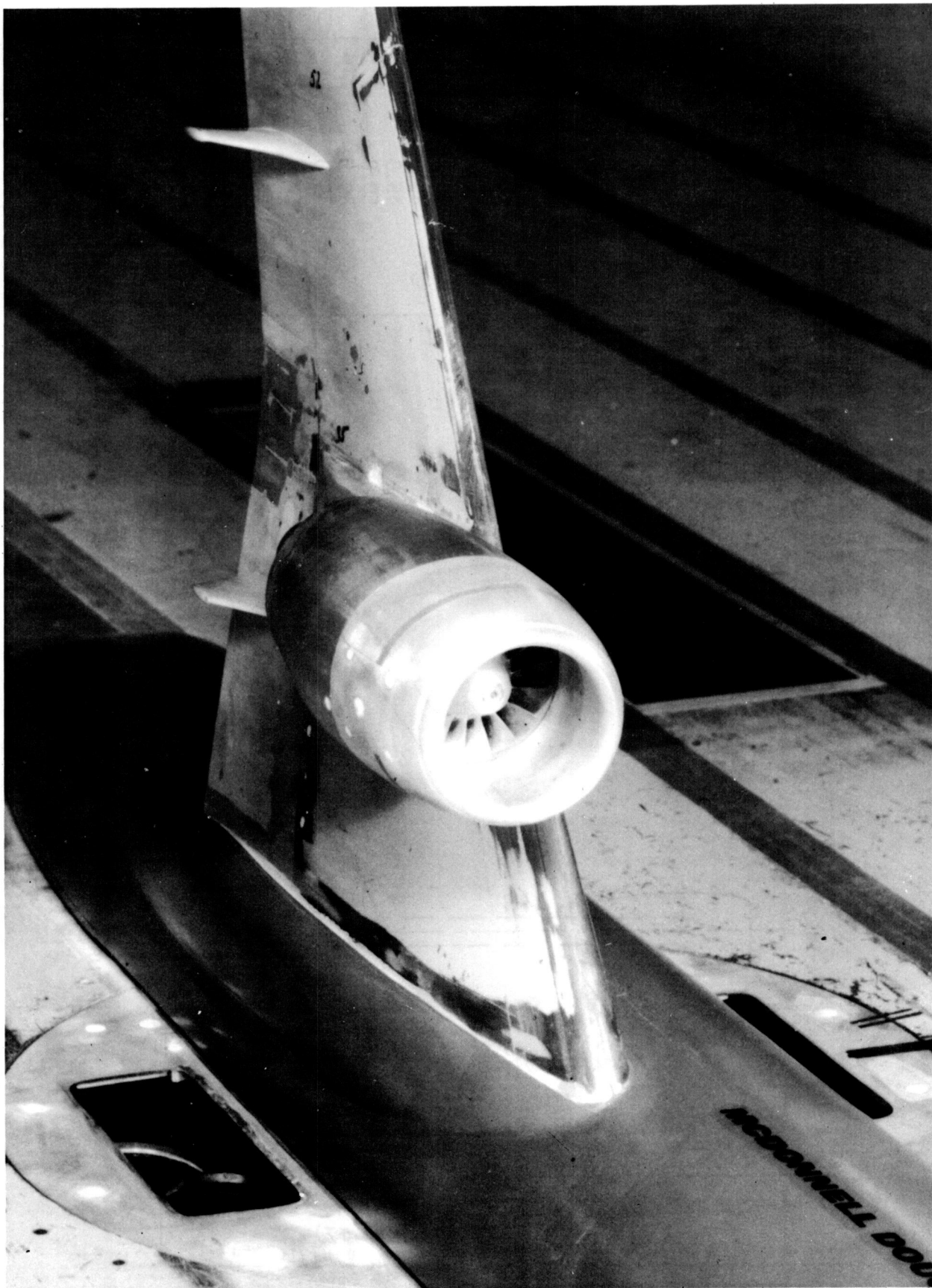
FIGURE 7. PHOTOGRAPH OF POWERED NACELLE INSTALLED ON WING

17
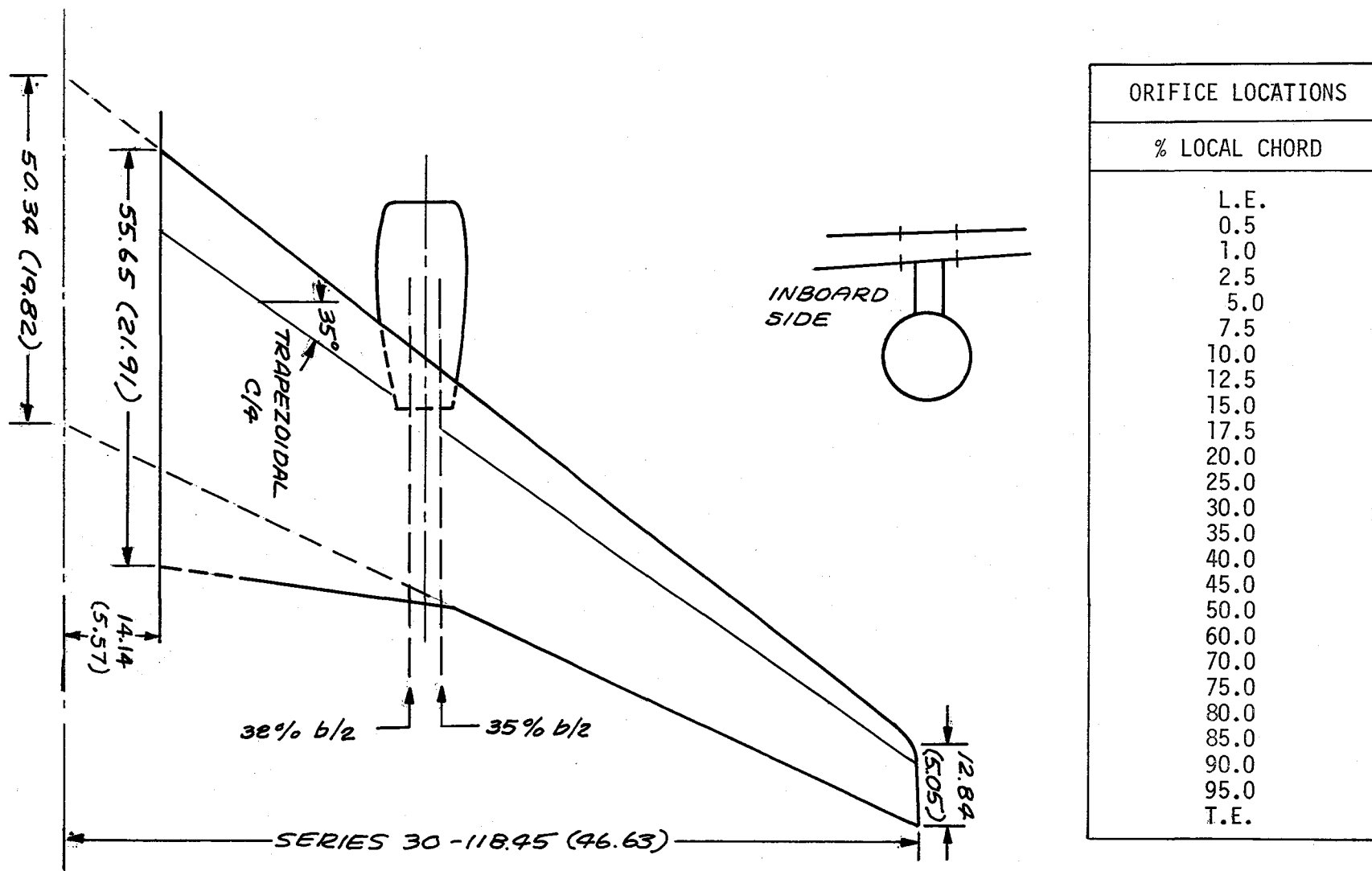
FIGURE 8. DC-10-30 WING GEOMETRY AND STATIC PRESSURE ORIFICE LOCATIONS

ORIFICE LOCATIONS
% LOCAL CHORD
L.E.
0.5
1.0
2.5
5.0
7.5
10.0
12.5
15.0
17.5
20.0
25.0
30.0
35.0
40.0
45.0
50.0
60.0
70.0
75.0
80.0
85.0
90.0
95.0
T.E.

50.34 (19.82)

55.65 (21.91)

35°

TRAPEZOIDAL C/4

14.14 (5.57)

INBOARD SIDE

32% b/2 — 35% b/2

12.84 (5.05)

SERIES 30 -118.45 (46.63)
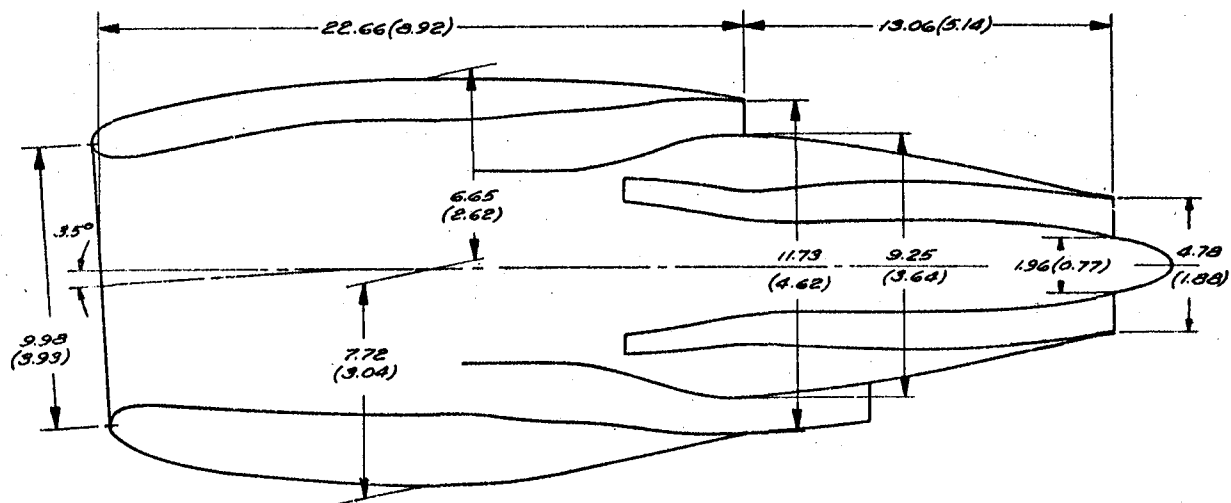
POWERED SDN

FLOW-THROUGH LDN
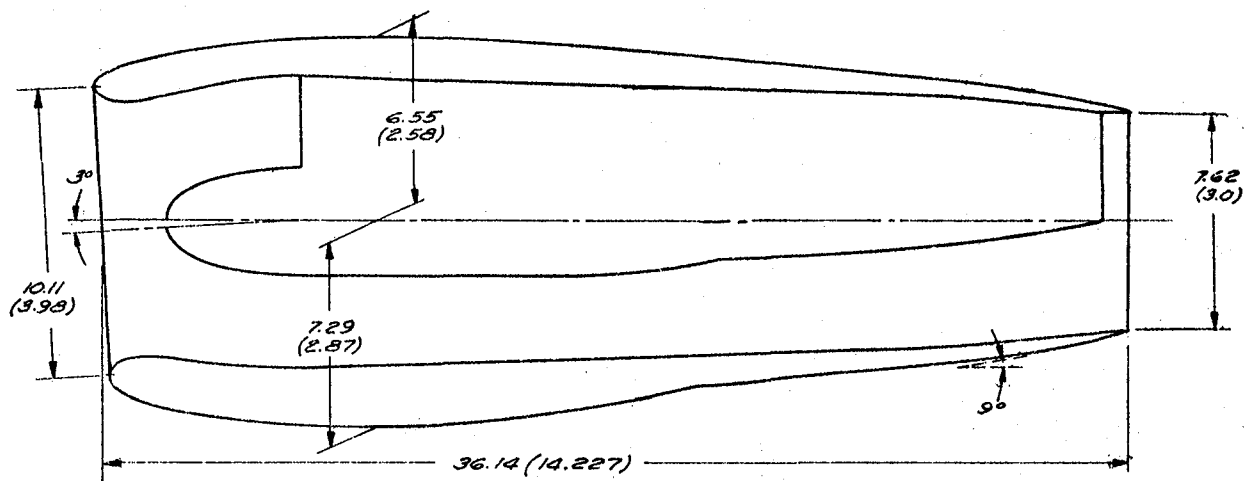
POWERED LDN
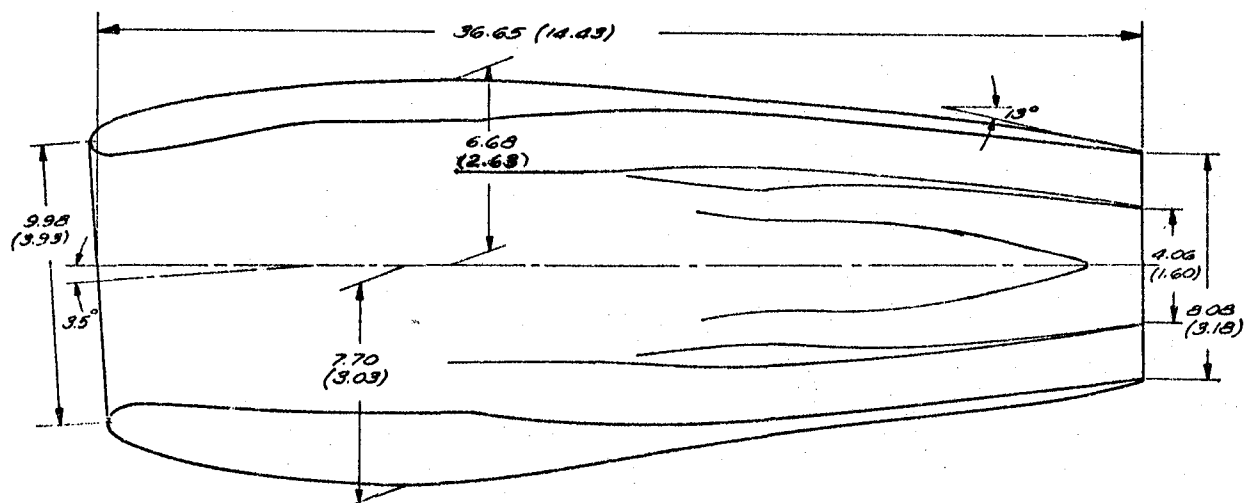
FIGURE 9. NACELLE MODEL GEOMETRIES

19

FLOW-THROUGH LDN

SCANIVALVE (332-48) FOR
NACELLE AND PYLON PRESSURES

POWERED LDN

DRIVE AIR LINE

INLET STATIC
PRESSURES

TURBO SIMULATOR ENGINE

POWERED SDN

DRIVE AIRLINE

INLET STATIC
PRESSURES

TURBO SIMULATOR ENGINE
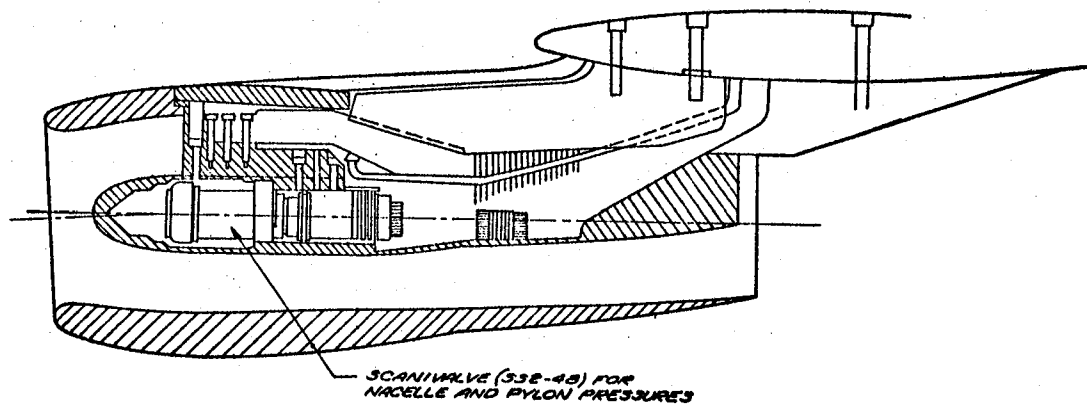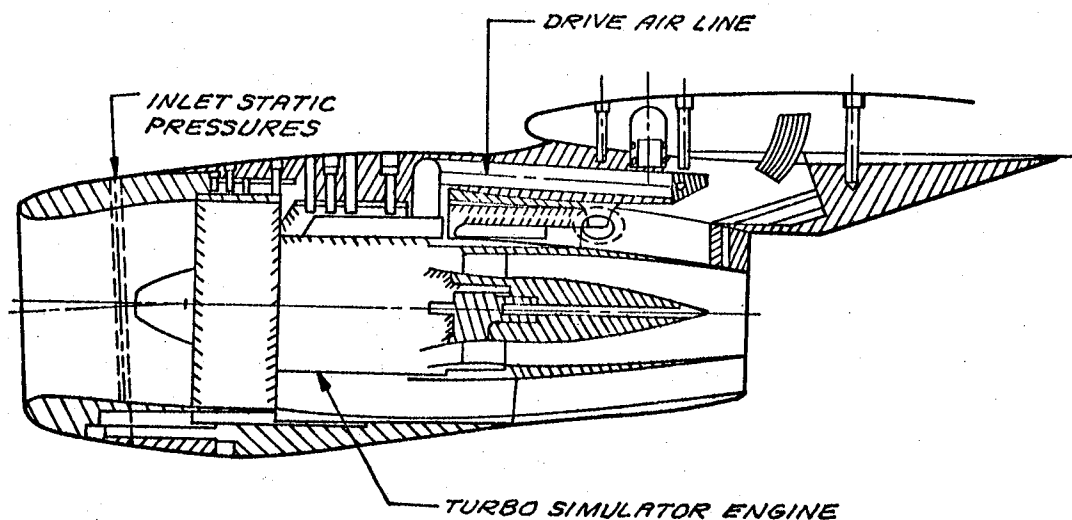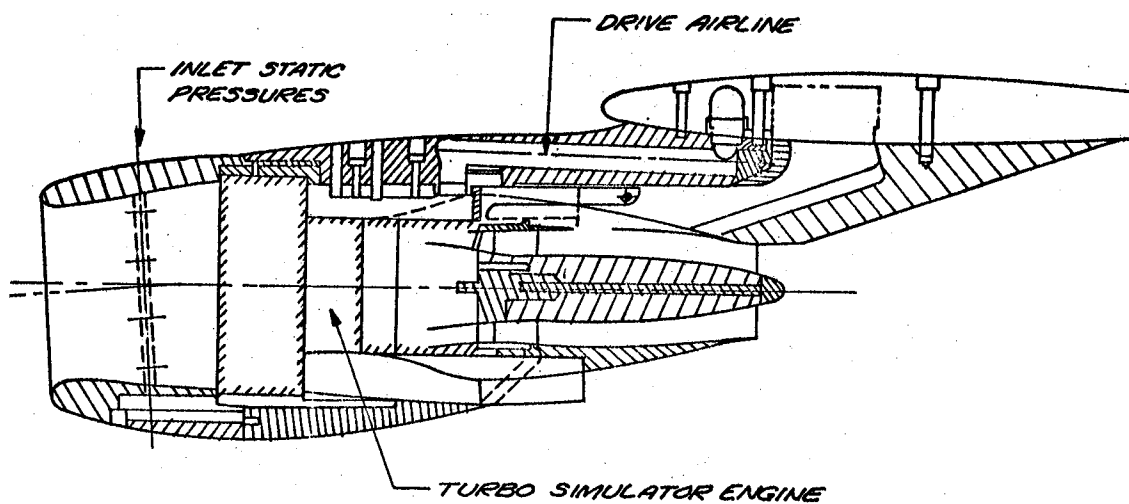
FIGURE 10. NACELLE MODELS INSTALLED ON WING

20

FLOW-THROUGH LDN
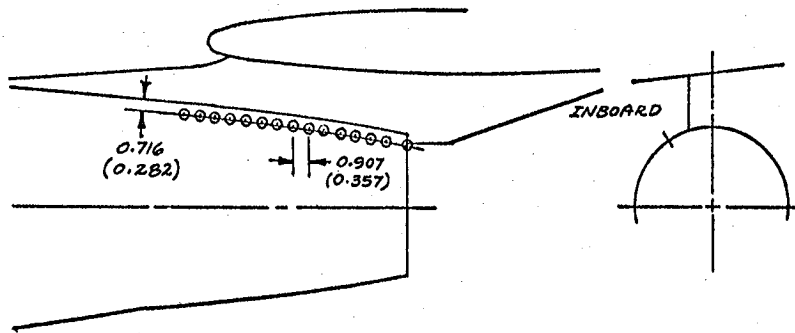
NACELLE ORIFICE LOCATION
% WING CHORD
-0.1
2.2
4.4
6.6
8.9
11.1
13.3
15.6
17.8
20.0
22.3
24.5
26.7
28.9
31.2

POWERED LDN
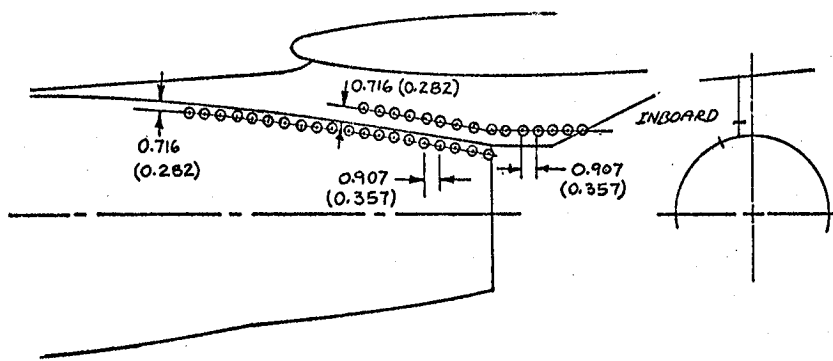
ORIFICE LOCATIONS	
% WING CHORD	
NACELLE	PYLON
-10.4	
-8.2	
-6.0	
-3.9	
-1.7	
0.5	
2.7	
4.9	
7.1	
9.3	
11.5	
13.6	13.6
15.9	15.9
18.0	18.0
20.2	20.2
22.4	22.4
24.6	24.6
26.8	26.8
29.0	29.0
31.2	31.2
	33.4
	35.6
	37.7
	39.9
	42.1
	44.3

POWERED SDN
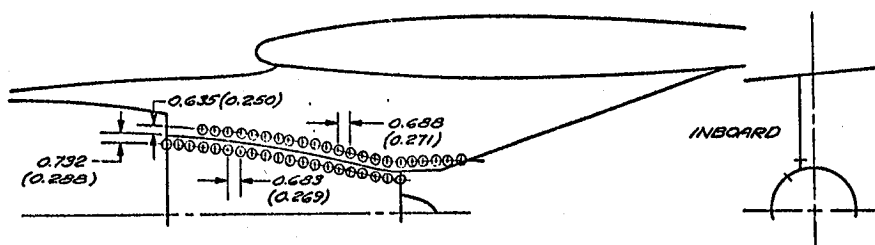
ORIFICE LOCATIONS	
% WING CHORD	
NACELLE	PYLON
-8.9	
-7.2	
-5.6	
-3.9	-3.9
-2.3	-2.3
-0.6	-0.6
1.0	1.1
2.7	2.7
4.3	4.4
6.0	6.1
7.6	7.7
9.3	9.4
10.8	11.0
12.5	12.7
14.2	14.4
15.8	16.0
17.5	17.7
19.1	19.4
20.8	21.0
22.5	22.7
	24.3
	26.0
	27.7
	29.3
	31.0

FIGURE 11. STATIC PRESSURE ORIFICE LOCATIONS ON NACELLES AND PYLONS

21

Two pylon fairings (Table 1) which were tested with the flow-through LDN are both contoured on the inboard side, with the large fairing pylon trailing edge located further aft than that of the small fairing pylon. The forward portion of these pylons is the same as the production pylon. Both pylons locate the LDN at the same location as for the baseline pylon. These pylon fairings are compared with the baseline symmetrical pylon in Figure 12. As shown in the figure, the pylons are instrumented with a row of static pressure orifices.

Boundary Layer Transition Strips - All testing was accomplished with transition fixed. Boundary layer transition strips of 0.318-cm (0.125-in.)-wide bands of glass beads were used on all components of the model. Full-span transition strips of 0.0081-cm (0.0032-in.)-diameter beads were placed 1.27 cm (0.5 in.) aft of the leading edge on the upper and lower surfaces of the wing. The fuselage was equipped with a strip of 0.0069-cm (0.0027-in.) beads located 3.175 cm (1.25 in.) aft of the nose. Transition strips of 0.0069-cm (0.0027-in.) beads were located on all pylons 0.254 cm (0.10 in.) aft of the pylon leading edge measured perpendicular to the leading edge. The flow-through LDN was equipped with strips of 0.0058-cm (0.0023-in.) beads located on the inside and outside surfaces of the inlet 0.508 cm (0.2 in.) from the inlet leading edge. The powered LDN had similar transition strips on the external surface only.

Test Conditions

The measurements were taken over a Mach number range of 0.60 to 0.84. For the isolated nacelle model test, all measurements were taken with the nacelle installed at zero angle of attack. A Reynolds number of 22.97 by 10^6 per meter (7.0 by 10^6 per foot) was held constant for the isolated nacelle tests. Analytical corrections for Reynolds number were applied to this nacelle drag for application to the semispan tests. For the semispan model test, the angle of attack of the model was varied from 1 to 4 degrees over a range corresponding to lift coefficient values between 0.30 to 0.60. The Reynolds number for the semispan test was reduced from that for the isolated nacelle test because it was not possible to achieve the required fan nozzle pressure ratios at high Reynolds number due to high pressure losses in the turbine

22
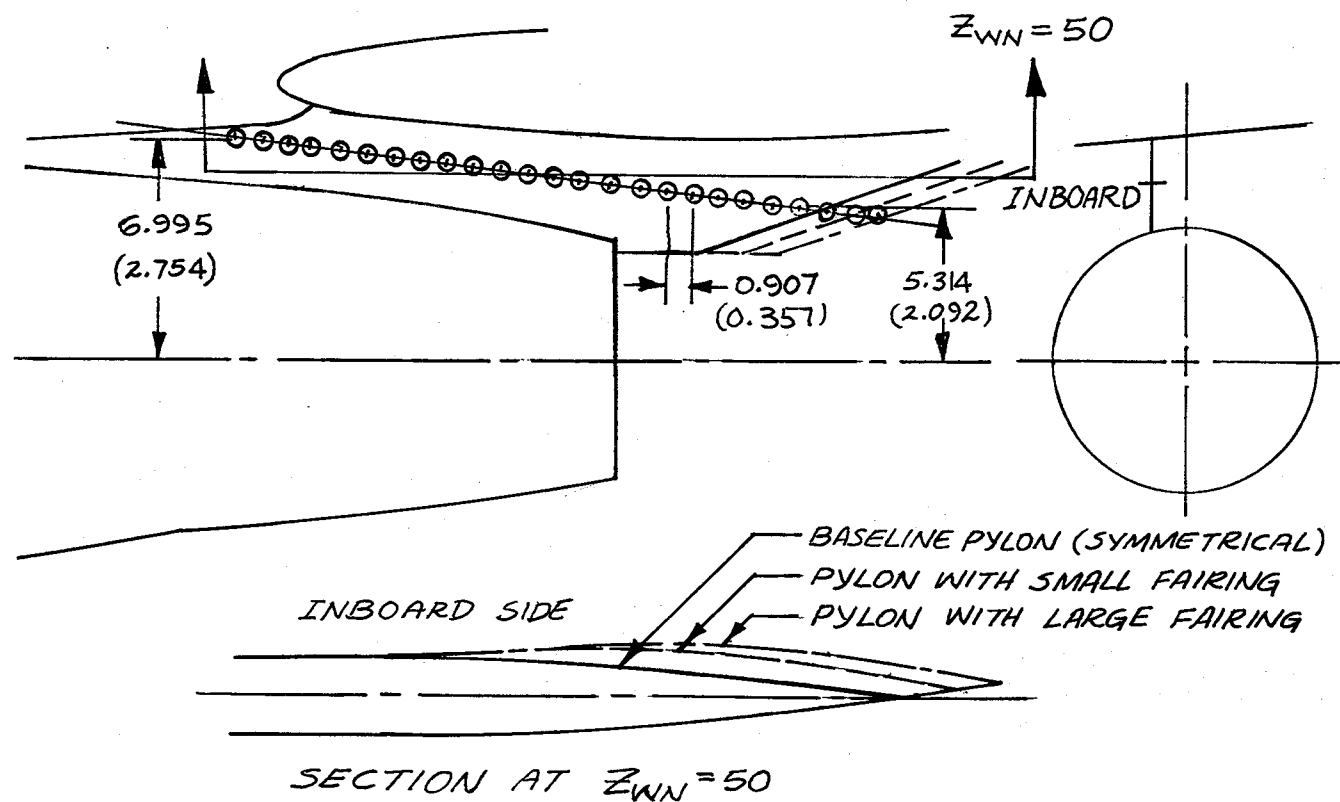
PYLON ORIFICE LOCATION		
% WING CHORD		
BASELINE	SMALL FAIRING	LARGE FAIRING
-0.1	-0.1	-0.1
2.2	2.2	2.2
4.4	4.4	4.4
6.6	6.6	6.6
8.8	8.8	8.8
11.0	11.0	11.0
13.3	13.3	13.3
15.5	15.5	15.5
17.7	17.7	17.7
20.0	20.0	20.0
22.2	22.2	22.2
24.4	24.4	24.4
26.6	26.6	26.6
28.9	28.9	28.9
31.1	31.1	31.1
33.3	33.3	33.3
35.5	35.5	35.5
37.8	37.8	37.8
40.0	40.0	40.0
42.2	42.2	42.2
44.4	44.4	44.4
46.7	46.7	46.7
	48.9	48.0
		51.1
		53.3

FIGURE 12. LDN PYLON CONFIGURATIONS AND STATIC ORIFICE LOCATIONS

drive air lines for the semispan model. A Reynolds number of 18.0×10^6 per meter (5.5×10^6 per foot) was held constant for the semispan model tests. The turbo-simulator was set at an RPM to simulate fan nozzle pressure ratios of 1.5 and 1.55, representative of cruise conditions for the DC-10-30.

Measurements

A five-component external balance was used to obtain the force and moment data during the isolated nacelle calibration and semispan model tests. Side-force measurements were not taken. The angle of attack was measured with a Douglas-furnished system which utilizes two linear potentiometers.

Chordwise static pressure distributions on the wing were measured at 32 percent and 35 percent on the top and bottom surfaces of the wing. Static pressure distributions were also measured on the nacelles and pylons on the inboard side at 0.72 cm (0.28 in.), model scale, from the nacelle-pylon juncture.

For the powered-nacelle model, in addition to the external surface static pressures, inlet static pressures, fan and turbine duct rake total and static pressures were measured. Measurements required for the turbo-simulator consisted of fan and turbine duct air temperature, drive air pressures, and the engine RPM.

All forces, moments, and pressures were recorded on the Ames wind tunnel data acquisition system. Photographs of fluorescent minitufts located on the inboard sides of the nacelles and pylons were taken at specified points during the test.

A summary of the test configurations is presented in Table 2.

TABLE 2
TEST PROGRAM SUMMARY

ISOLATED NACELLE CALIBRATION TEST			
CONFIGURATION	PYLON	θ_{NAC}	PURPOSE
STRUT + POWERED SDN	BASE	0°	To calibrate nacelles for semispan test
STRUT + POWERED LDN	BASE	0°	
STRUT + LDN	BASE	0°	To obtain isolated nacelle drag

SEMISPAN MODEL TEST			
CONFIGURATION	PYLON	$\Delta\theta_{NAC}$	PURPOSE
WING-BODY (WB)	—	—	To obtain wing-body reference baseline
WB + POWERED SDN	BASE	BASE	Base for determining interference drag difference, LDN-SDN
WB + LDN	BASE	BASE	To assess interference drag due to installation of LDN
WB + LDN	BASE	$+1.5^\circ$	To evaluate effect of nacelle incidence angle
WB + LDN	BASE	-1.5°	
WB + LDN	SMALL FAIRING	BASE	To reduce interference drag, if any, due to installation of LDN
WB + LDN	LARGE FAIRING	BASE	
WB + POWERED LDN	BASE	BASE	To evaluate LDN power effects

Test Procedure

The following test procedure was used to determine wing-nacelle interference drag:

1. The isolated nacelle and pylon drag was determined as the difference between the nacelle plus pylon plus strut drag minus the strut tare drag.

2. Drag characteristics of the wing-body were measured.

3. Drag characteristics of the complete semispan model were measured.

4. The excess installation drag, or interference drag, was the difference between the complete semispan model drag coefficient and the addition of the wing-body plus isolated nacelle plus pylon drag coefficient compared at constant lift coefficient.

The isolated nacelle and pylon was calibrated at 0-degree angle of attack. The isolated data were not corrected for the internal drag of the nacelle.

Accuracy of Data

The Reynolds number was held to within ±328,000 per meter (±100,000 per foot) and the Mach number to within ±0.002 of the specified value.

Data for the wing-body alone and with the flow-through LDN installed were quite repeatable with little scatter.

After several configurations were tested, a small but significant angle of attack system malfunction was discovered. The sensitivity of measurements of drag to angle of attack system error is approximately 1 percent of airplane drag per 0.03 degree of error. Several angle of attack system components (Douglas and NASA) were replaced and most of the configurations were repeated. During the remainder of the test, the indicated angle of attack was carefully monitored. The system appeared to still experience a small residual drift. A correction was devised, based on diagnostic run procedures and static calibration data, and was applied prior to analysis of the data. The

resulting scatter and repeatability were within one to two drag counts. The corrections were small and the repeatability of the drag polars was such that omitting the drift corrections would not change any of the conclusions of this report.

A significant amount of effort was expended to evaluate the powered nacelle data. The quality of the drag polars was much poorer than for the flow-through data. The absolute drag levels shifted and significant differences in both favorable and unfavorable interference drag appeared to occur at 0.60 Mach number. At 0.60, all configurations should be free of compressibility effects and, therefore, the interference drag should be zero.

The problems associated with the powered nacelle data are probably related to the calculation of simulator thrust. To determine interference drag involves determining a power-off drag polar, which requires calculating simulator thrust from the calibration data. The major problem for the powered nacelle was the contamination of internal pressure instrumentation by oil leakage. This occurred because of over oiling (in retrospect) of the turbo-simulator following a bearing failure early in the test program. A sizable study was done to attempt to identify the noncontaminated pressure probes in order to calculate fan and turbine pressure ratios. This approach was not satisfactory as the fan pressure ratios drifted for a given RPM and drive overflow. Thus it was not possible to determine the engine thrust correctly. An alternate approach to determine turbo-simulator thrust was to use engine RPM. However, an examination of this technique showed it did not yield satisfactory results (i.e., did not properly account for changes in nozzle discharge coefficients). It was concluded that the powered model force data were irretrievable and not of sufficient accuracy to draw any conclusions. For these reasons, force data conclusions are based only on the flow-through nacelle force data. Wing-pylon-nacelle channel pressure data are used to assess the power effects on the LDN installation.

RESULTS AND DISCUSSIONS

Typical cruise conditions for the international versions of the DC-10 are
0.82 Mach number at 0.50 lift coefficient (C_L) with step climbs occurring at
0.45 and 0.54 lift coefficients. As these conditions band the cruise regime,
data comparisons are presented for these lift coefficients. The test con-
figurations were also evaluated at lower Mach numbers (0.6 the lowest) to
determine the effects of compressibility. Where appropriate, configuration
comparisons are shown as a function of Mach number.

Isolated Nacelle Calibration

The drag coefficient of the isolated flow-through LDN and symmetrical pylon
is shown in Figure 13. The drag coefficient (including internal drag) is
nearly a constant 20 counts (C_D = 0.0020) and independent of Mach number.
The drag coefficient was used to evaluate wing-nacelle interference drag
for the flow-through LDN.

Semispan Model

Baseline Long-Duct Nacelle - The interference drag characteristics for the
flow-through LDN with the baseline symmetrical pylon are shown in Figure 14.
Nominal cruise conditions are 0.82 Mach number at 0.50 lift coefficient.
However, since step climb occurs at lower lift coefficients and the wing
lower surface velocities (peak negative pressures) increase with decreasing
lift coefficient, the interference drag coefficients are shown at 0.50 and
lower lift coefficients.

At M_∞ = 0.82 and C_L = 0.50 (Figure 14), the interference drag coefficient
is about 0.00015 ($\approx$ 1/2 percent of airplane drag) and does not show a
significant Mach number dependency. At C_L = 0.40 and 0.45, the interference
drag coefficient was smaller at most subsonic Mach numbers but showed more
pronounced Mach number dependency at the higher Mach numbers. Although
outside the lift coefficient range for normal cruise conditions, the inter-
ference drag characteristics (not shown here) were also examined for lift
coefficients as low as 0.30 to determine criticality to increasing channel
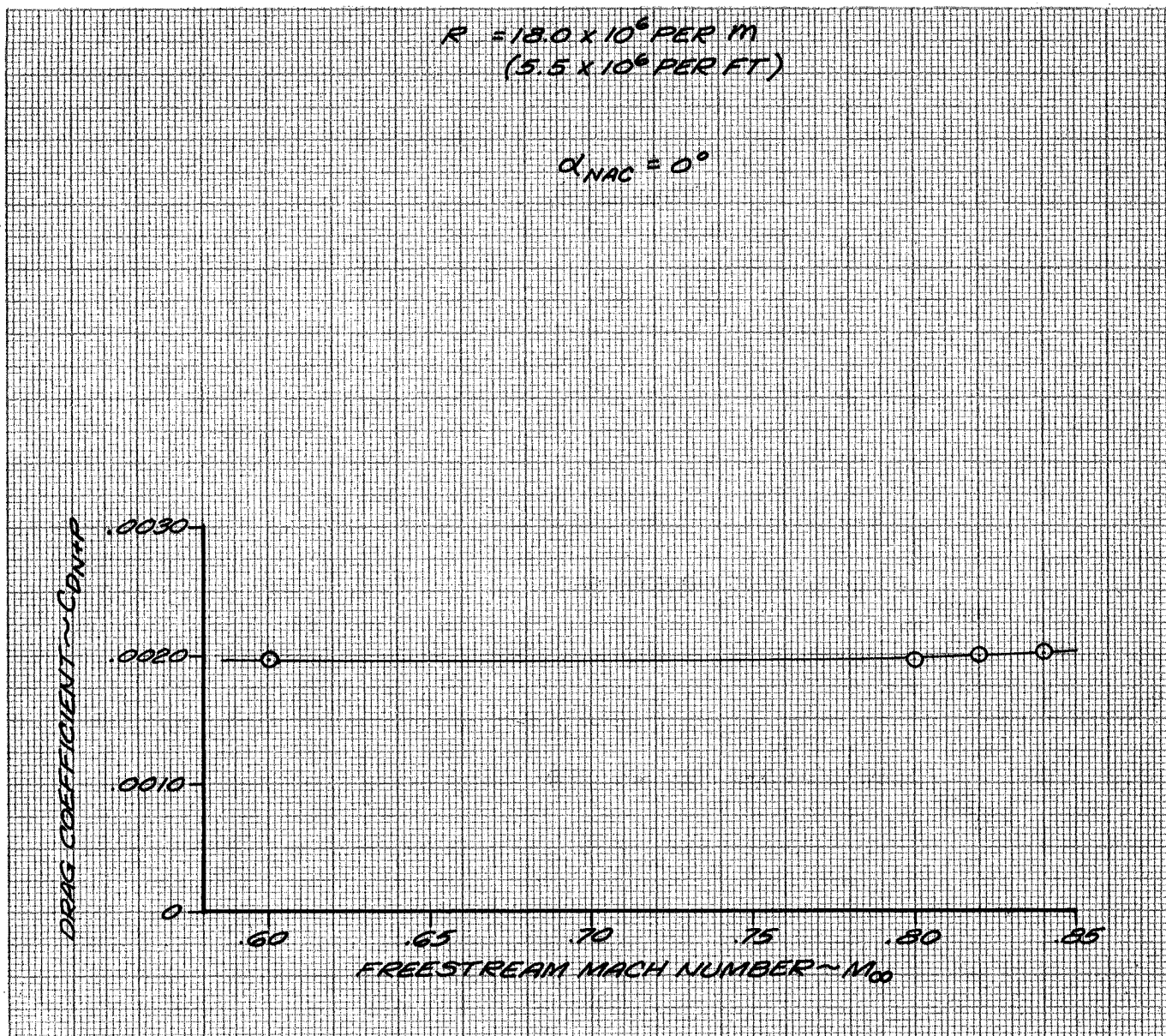velocities. The drag increment at 0.82 Mach number showed little, if any,

29

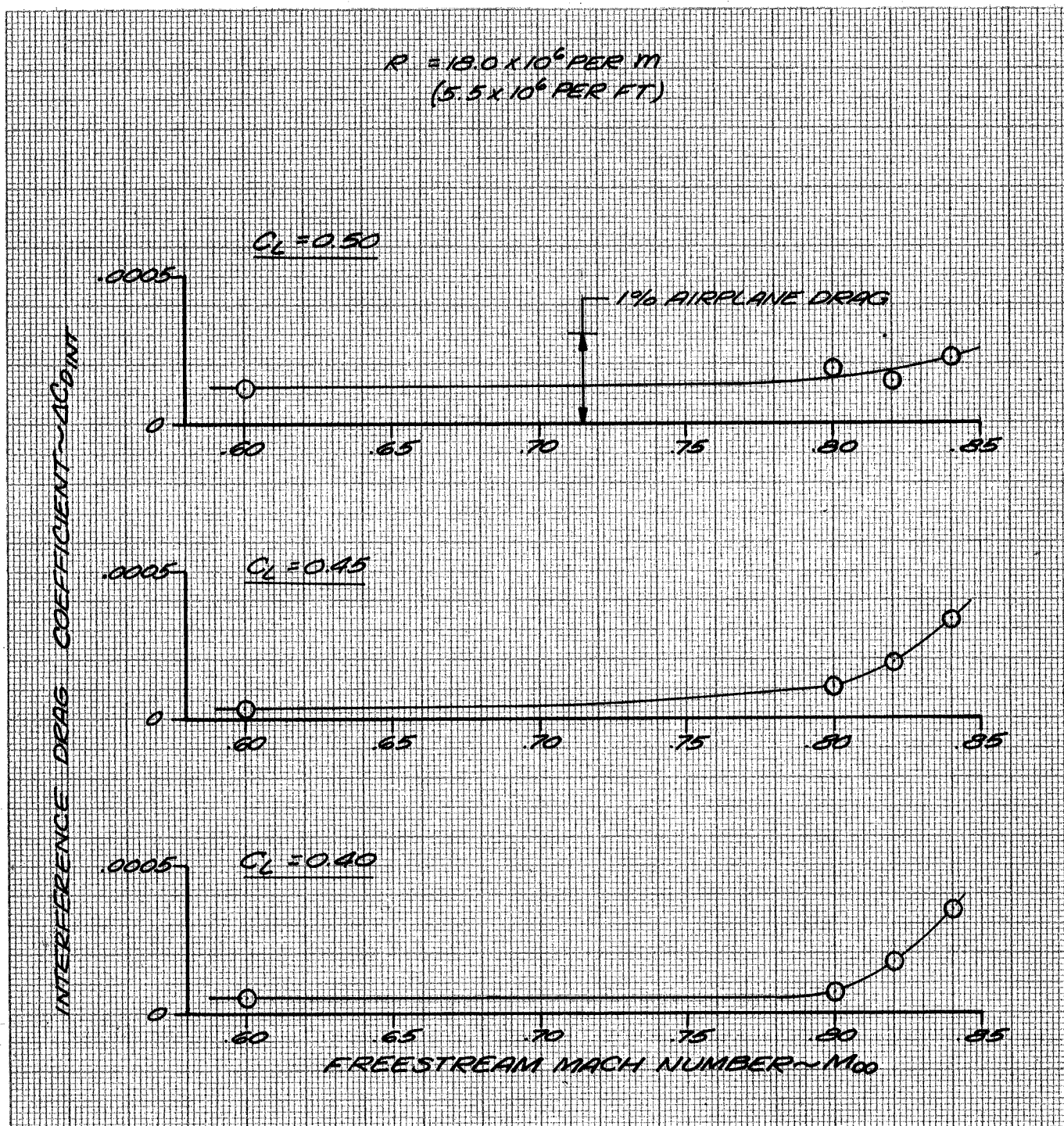FIGURE 13. ISOLATED FLOW-THROUGH LDN AND PYLON DRAG

30

FIGURE 14. INTERFERENCE DRAG CHARACTERISTICS FOR FLOW-THROUGH LDN WITH BASELINE SYMMETRICAL PYLON

31

lift coefficient dependency. The fact that there is a slight drag increment at 0.6 Mach number probably indicates the accuracy of the test apparatus, since the channel pressures are subcritical and show no indications of problems.

The flow-through LDN inboard wing-pylon-nacelle channel pressures are shown in Figures 15 through 18. At 0.6 Mach number, the channel flow is subcritical (Figure 15). Figure 16 shows that the flow in the channel is characterized by a growth in the peak suction pressures with increasing Mach number. The channel flow becomes critical at about 0.8 Mach number resulting in a peak local Mach number across the channel of about 1.1 at the cruise condition of 0.82 freestream Mach number.

Figures 17 and 18 show the complete channel pressure distributions. The wing lower surface pressure distribution is also shown without the nacelle installed. The peak negative suction pressures are about 0.2 to 0.3 higher with the nacelle installed. However, the peak channel Mach number is well below the Mach = 1.3 to 1.4 levels which have been known to cause shock-induced nacelle flow separation and an attendant drag penalty on the DC-8 prototype LDN. Further, tuft observations on the LDN afterbody and pylon show complete flow attachment.

To further evaluate these data and to check how close the flow is to separation on the nacelle afterbody, a boundary layer analysis was undertaken using the wind-tunnel-measured afterbody pressure distributions. Figure 19 shows the wing-pylon-nacelle pressure distribution for the production SDN at cruise conditions. The peak suction pressures for this model in the Ames facility did not show the regions of separated flow on the CF6-50 installation as has been measured by DC-10-30 flight tests. Peak suction coefficients of about -0.1 higher have been measured for the SDN installation in flight and in another wind tunnel facility. Therefore, it was deemed appropriate to apply a correction to the LDN measured pressure distributions to account for this possible measurement error. The estimated LDN flight conditions were obtained by increasing the wind-tunnel-measured peak suction pressure coefficients by $\Delta C_p = -0.1$ and assuming a Reynolds number consistent with $M_\infty = 0.82$, 35,000 feet altitude. Results of this analysis, shown in Figure 20, do not show any tendency toward flow separation on the nacelle
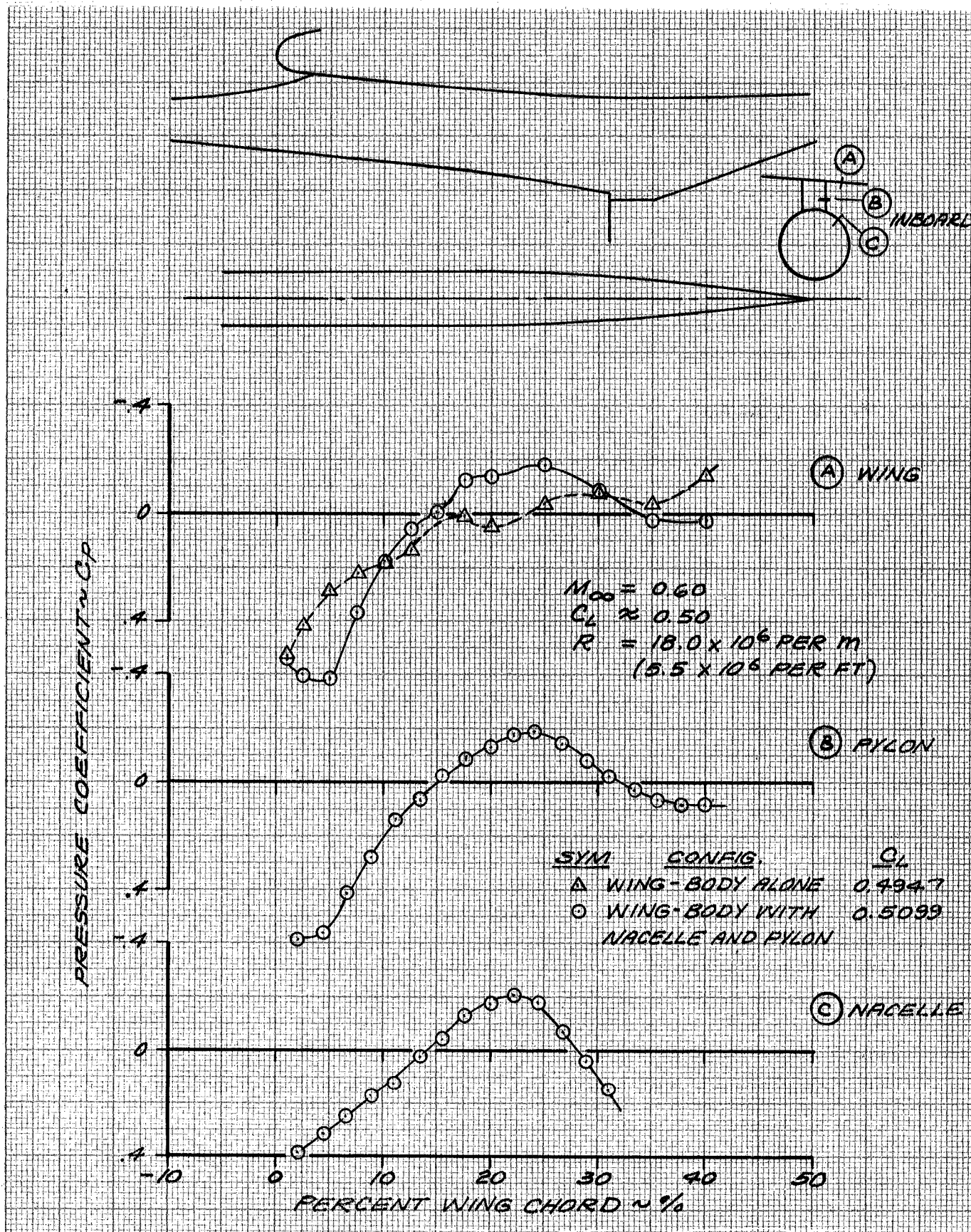
FIGURE 15. EFFECT OF LDN INSTALLATION ON INBOARD CHANNEL PRESSURES — BASELINE
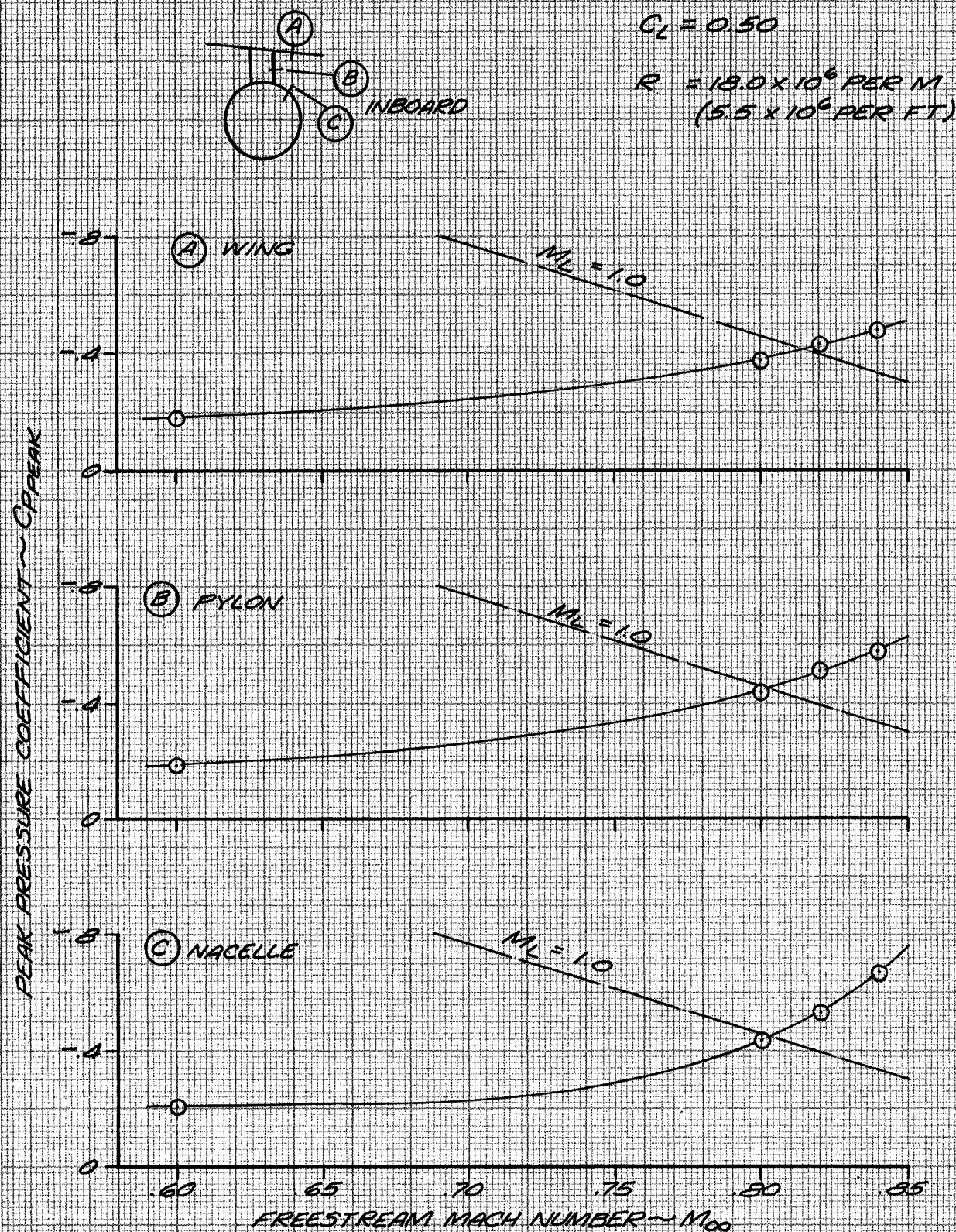SYMMETRICAL PYLON ($M_\infty = 0.60$, $C_L = 0.50$)

33

FIGURE 16. EFFECT OF FREESTREAM MACH NUMBER ON CHANNEL PEAK SUCTION
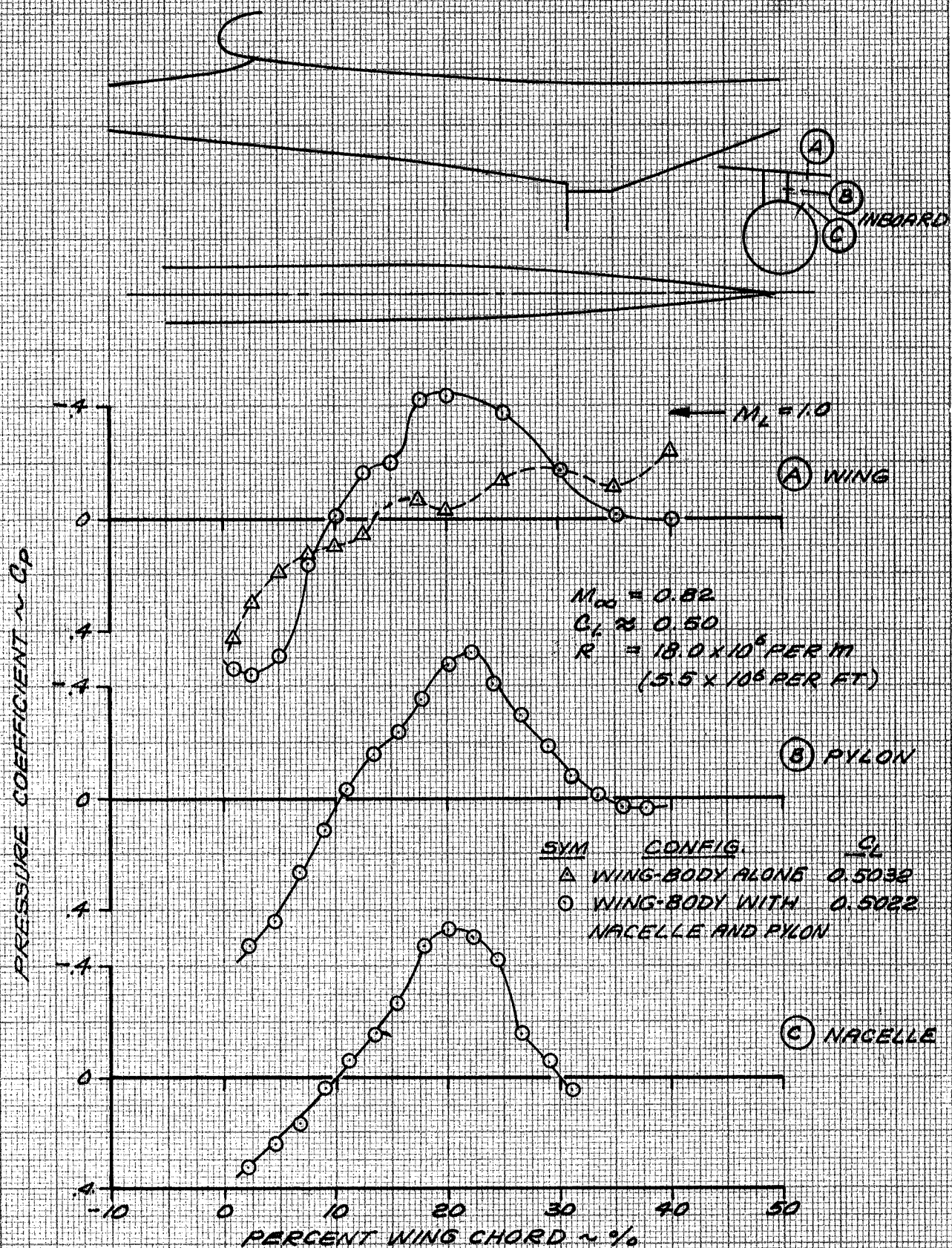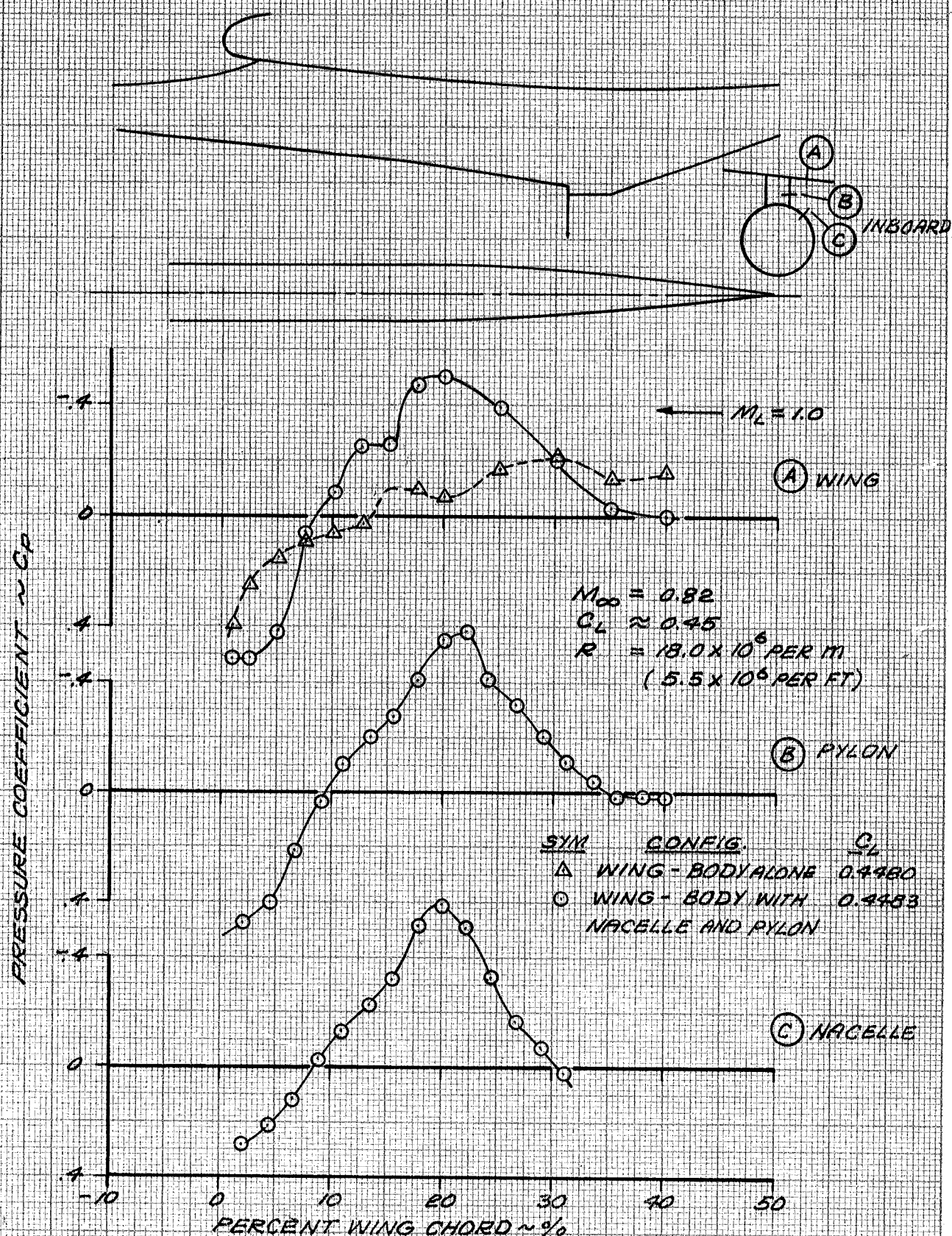PRESSURES – LDN WITH BASELINE SYMMETRICAL PYLON (C_L = 0.50)

34

FIGURE 17. EFFECT ON LDN INSTALLATION ON INBOARD CHANNEL PRESSURES – BASELINE SYMMETRICAL PYLON ($M_\infty = 0.82$, $C_L = 0.50$)

$\alpha_F = 3.2°$

35

$\alpha_W = 3.9°$

$\alpha_n = 4.8°$

FIGURE 18. EFFECT OF LDN INSTALLATION ON INBOARD CHANNEL PRESSURES — BASELINE
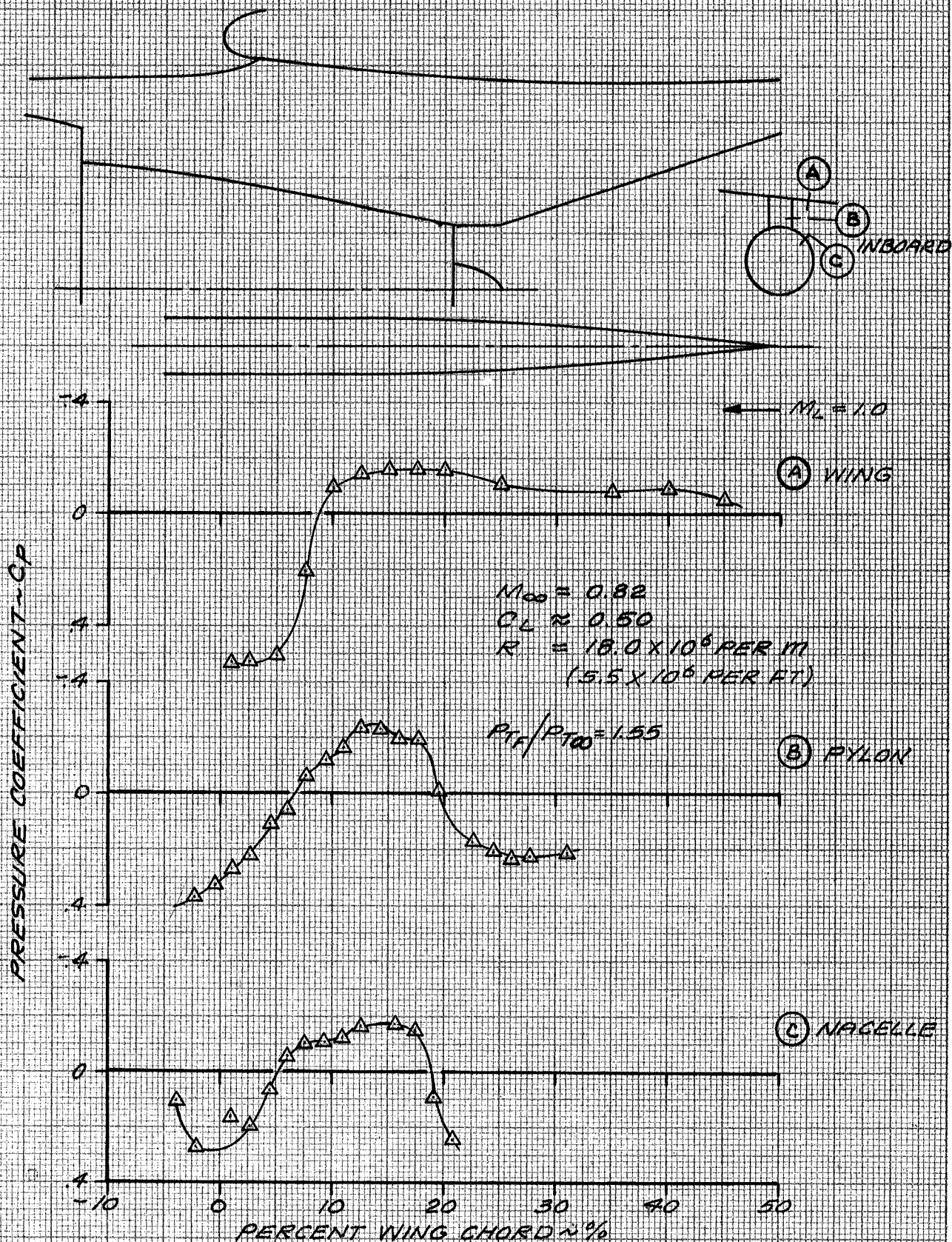SYMMETRICAL PYLON ($M_\infty = 0.82$, $C_L = 0.45$)

36

$\alpha_F = 2.7°$

$\alpha_W = 3.4$

$\alpha_n = 4.30°$

FIGURE 19. INBOARD CHANNEL PRESSURE DISTRIBUTIONS WITH POWERED PRODUCTION SDN
($M_\infty = 0.82$, $C_L = 0.50$)
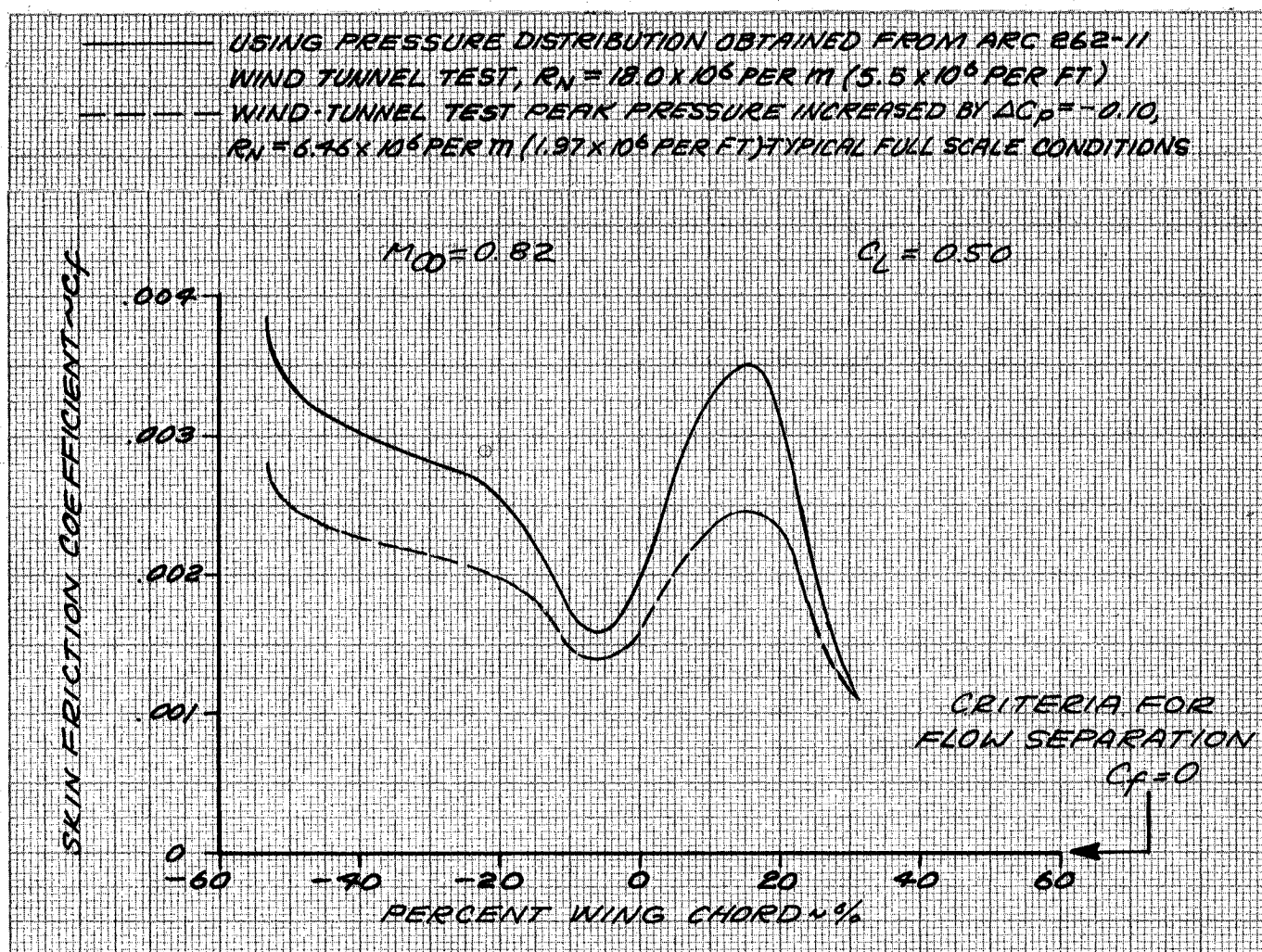
$\alpha = 8.2°$

37

FIGURE 20. PREDICTED SKIN FRICTION COEFFICIENT ON LDN AFTERBODY (M_∞ = 0.82, C_L = 0.50)

afterbody at either wind tunnel test conditions or flight conditions. Flow separation by the Cebeci criteria (Reference 6) would be indicated when the skin friction coefficient reaches zero.

The effects of power simulation on the inboard channel pressures at $M_\infty = 0.82$ are shown in Figure 21. The comparison is for the flow-through and powered LDN installations with baseline symmetrical pylon. The powered nacelle fan pressure ratio was 1.55 (NPR $\approx$ 2.4). Essentially no difference in either the peak suction pressures or the pressure gradients is indicated at any location across the channel. It is therefore concluded that for the LDN, power effects do not change the channel flow mechanism. Further, this implies that the flow-through LDN force results are directly applicable because any interference mechanisms are not power-dependent.

The effects of the nacelle and pylon on the airplane lift curve are shown in Figure 22. At typical cruise conditions the nacelle and pylon causes a loss in life of $\Delta C_L = -0.02$ relative to the wing body at the same angle of attack. This loss in lift is about the same for both the LDN and the SDN and is in good agreement with the increment that has been measured in past tests. Figure 23 shows the span load distribution at $M_\infty = 0.82$ and 3.2 degrees angle of attack. This condition corresponds to 0.5 C_L with the nacelle and pylon installed. For the configuration with the nacelles and pylons installed (LDN and SDN) wing pressures were available only at stations 32 and 35 percent of semispan, just inboard and outboard of the pylon. A pronounced loss in lift is seen at the inboard station while a slight loss in lift is seen at the outboard station. The loss in lift is caused primarily from increased suction pressure peaks on the wing lower surface inboard of the pylon.

Nacelle Incidence Angle - The effects of increased and decreased LDN incidence angle relative to that of the production SDN are shown in Figures 24 through 26. Figure 24 shows that angle change of ±1.5 degrees from the current nacelle incidence of 0.9 degree resulted in drag increases of approximately $C_D = 0.0002$ (2/3 percent airplane drag) at a cruise lift coefficient of 0.50. At 0.45 lift coefficient, the drag increase was about $C_D = 0.0003$ (1.0 percent airplane drag). The wing-pylon-nacelle channel pressures (Figures 25 and 26) indicate that the channel is slightly less critical with either increased or decreased nacelle incidence angle suggesting that the drag penalty is
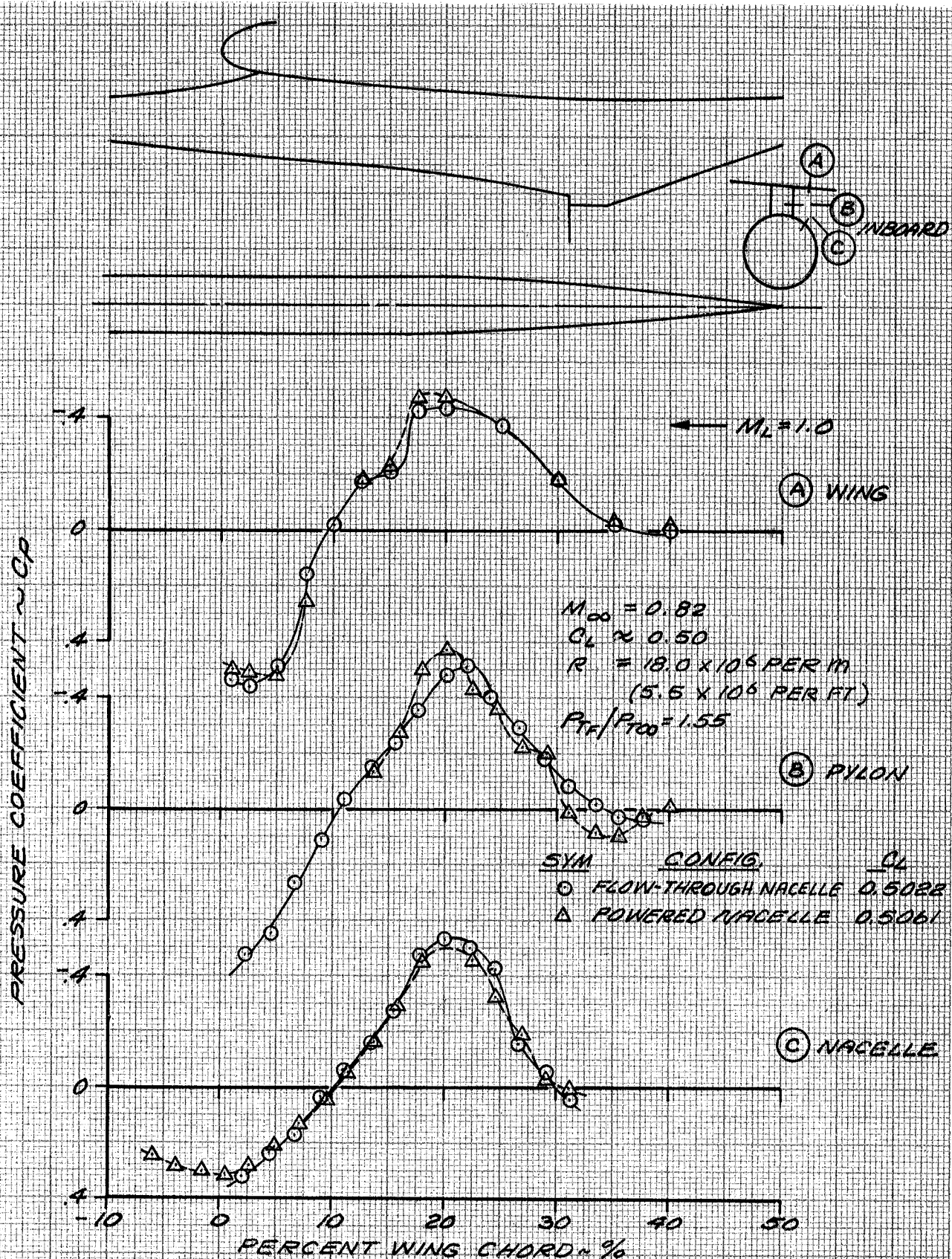
FIGURE 21. EFFECT OF POWER SIMULATION ON INBOARD CHANNEL PRESSURES — LDN WITH BASELINE SYMMETRICAL PYLON (M_∞ = 0.82, C_L = 0.50)
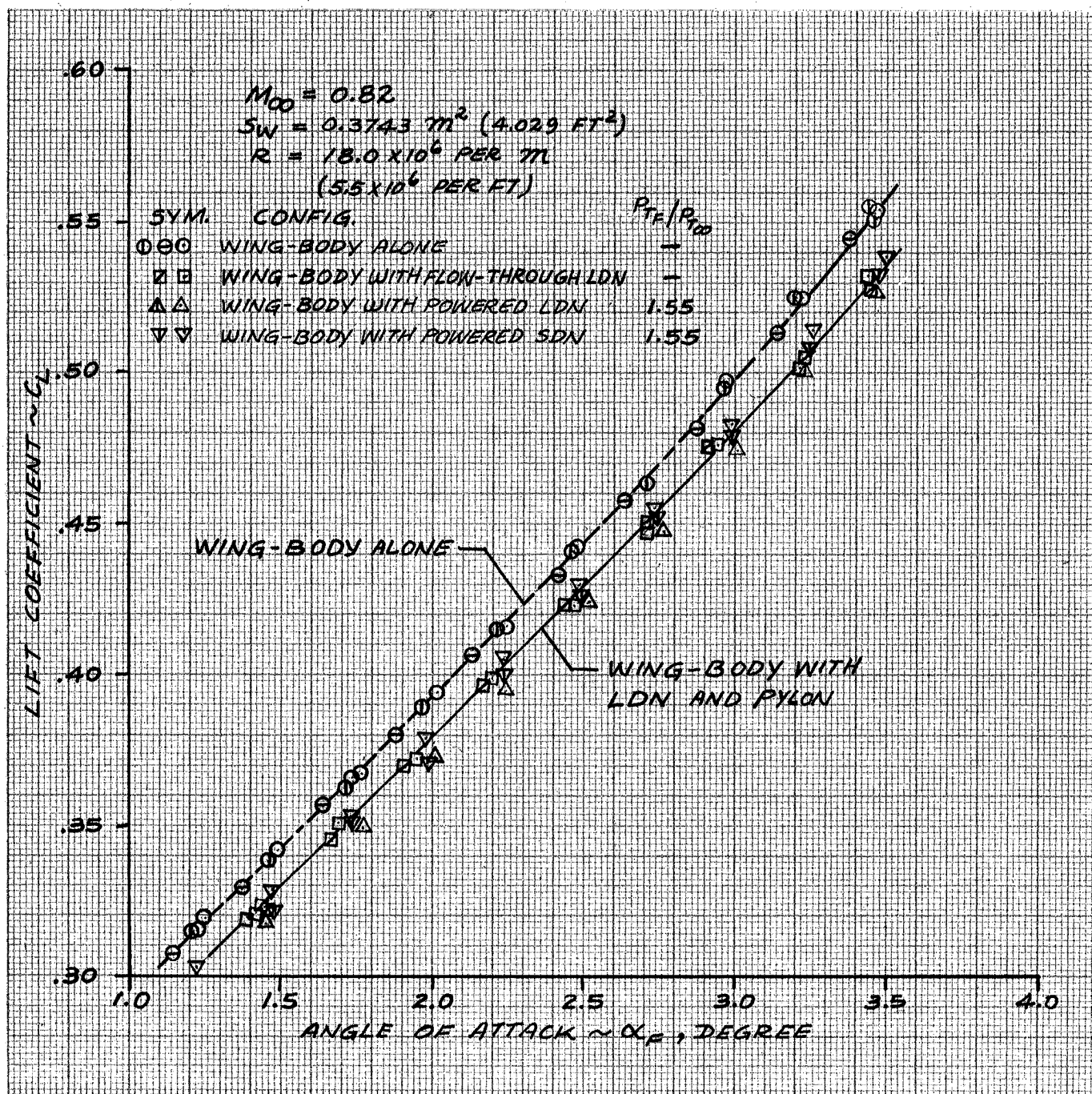
FIGURE 22. LIFT CURVES FOR WING-BODY WITH AND WITHOUT NACELLES AND BASELINE
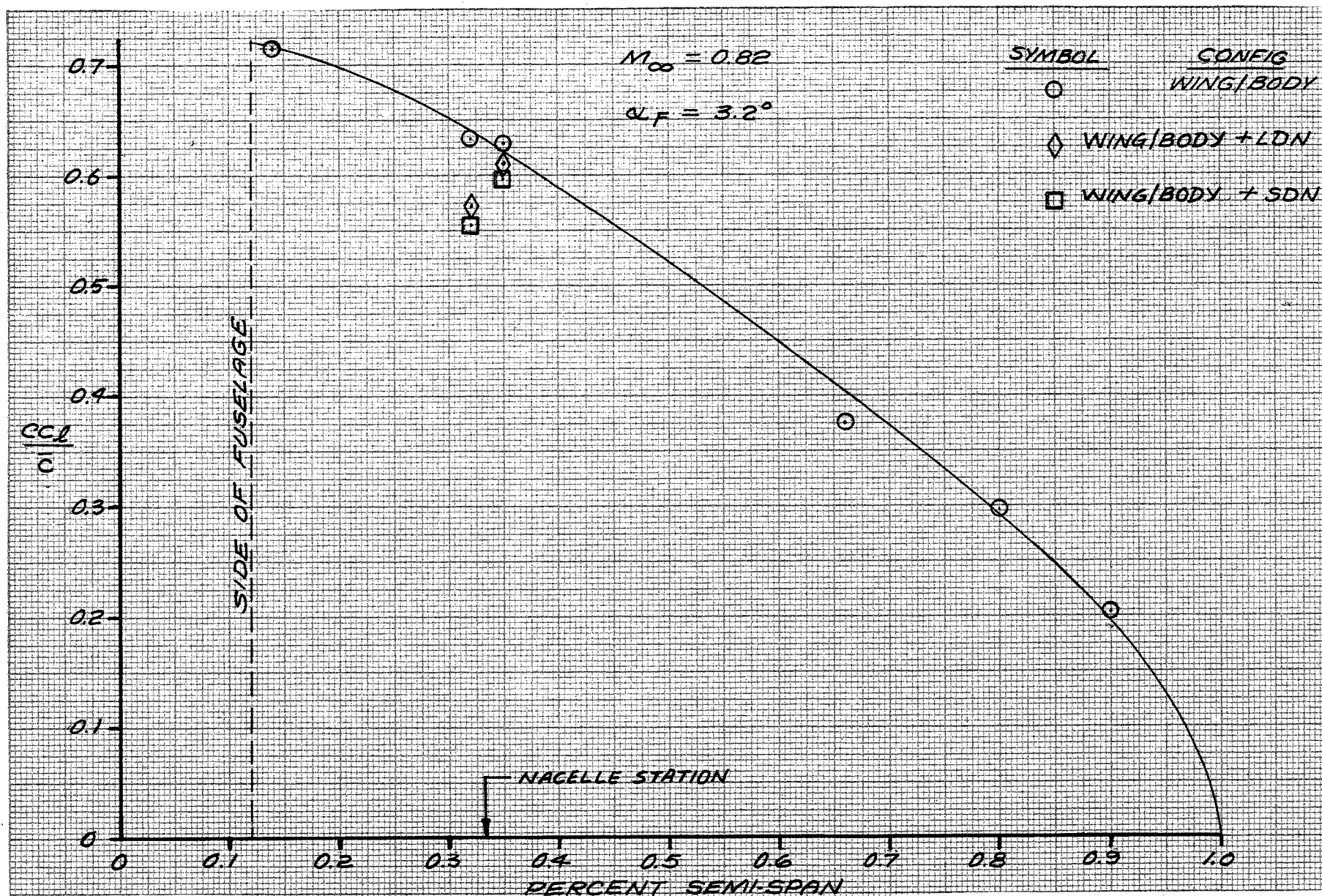SYMMETRICAL PYLONS (M_∞ = 0.82)

41

FIGURE 23. SPANLOAD DISTRIBUTION WITH AND WITHOUT NACELLES AND PYLONS
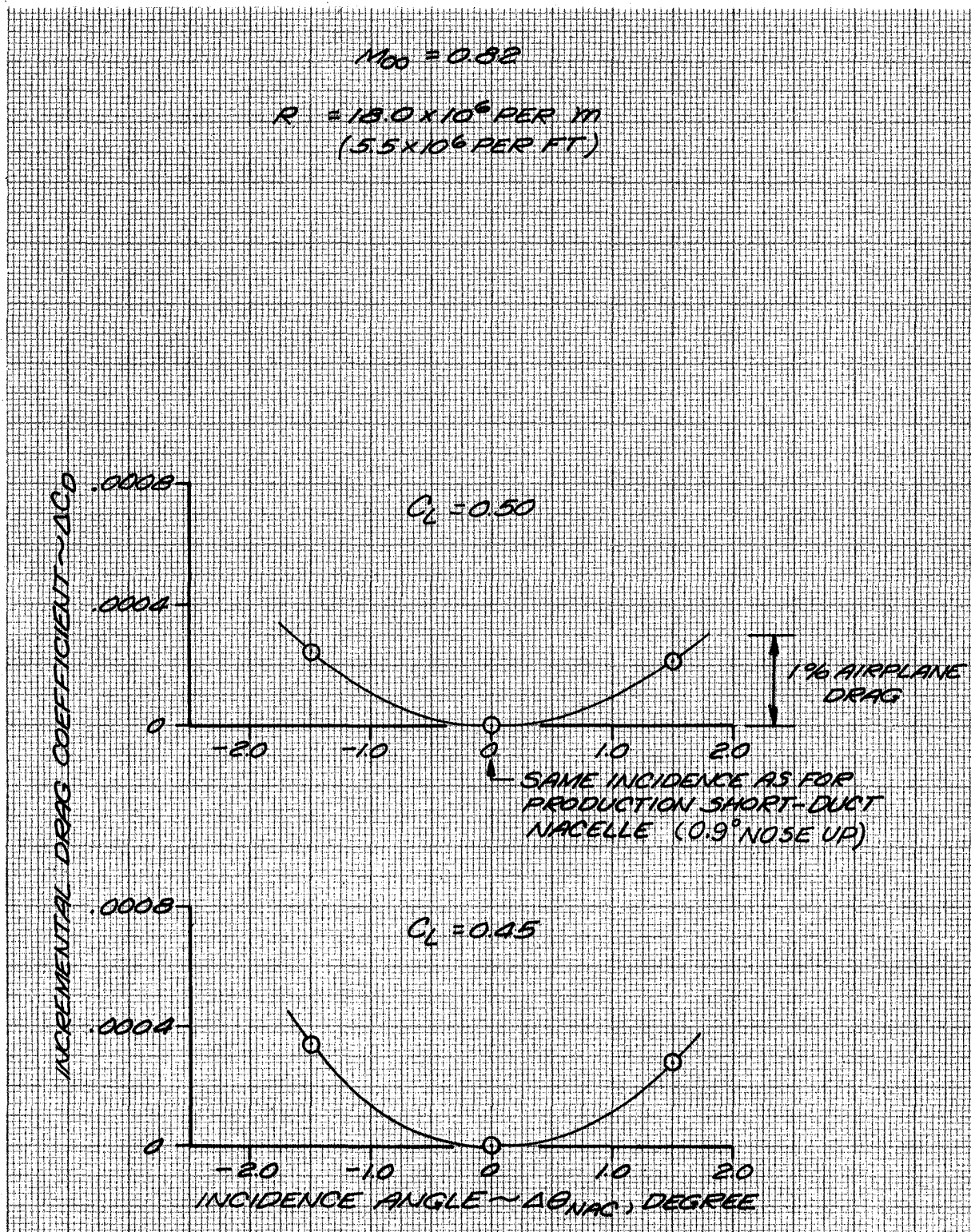(M_∞ = 0.82, α_F = 3.2º, $C_L \approx$ 0.50)

FIGURE 24. EFFECT OF NACELLE INCIDENCE ANGLE CHANGE ON INCREMENTAL DRAG —
FLOW-THROUGH LDN WITH BASELINE SYMMETRICAL PYLON (M_∞ = 0.82)
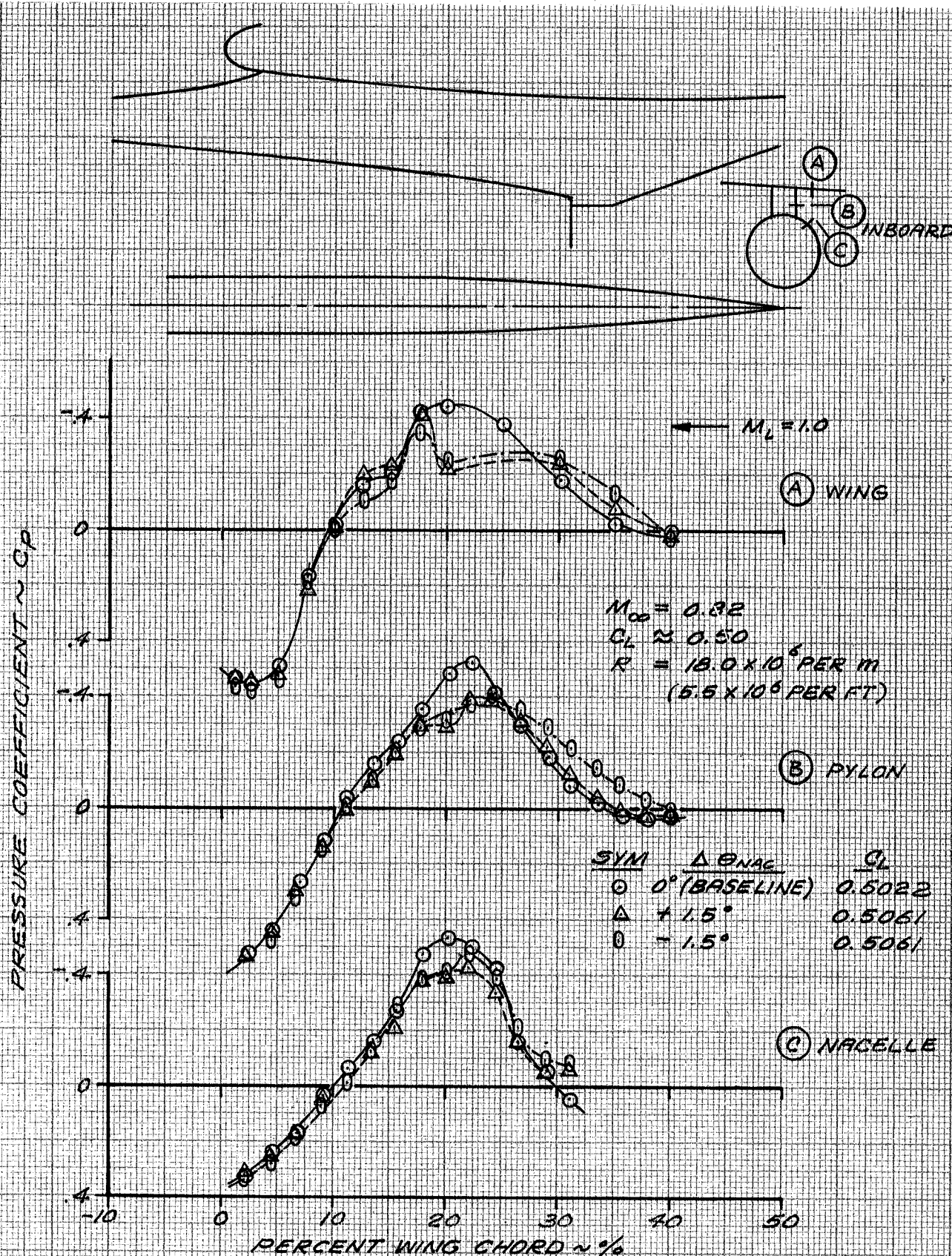
43

FIGURE 25. EFFECT OF NACELLE INCIDENCE ANGLE CHANGE ON INBOARD CHANNEL
PRESSURES — FLOW-THROUGH LDN WITH BASELINE SYMMETRICAL PYLON
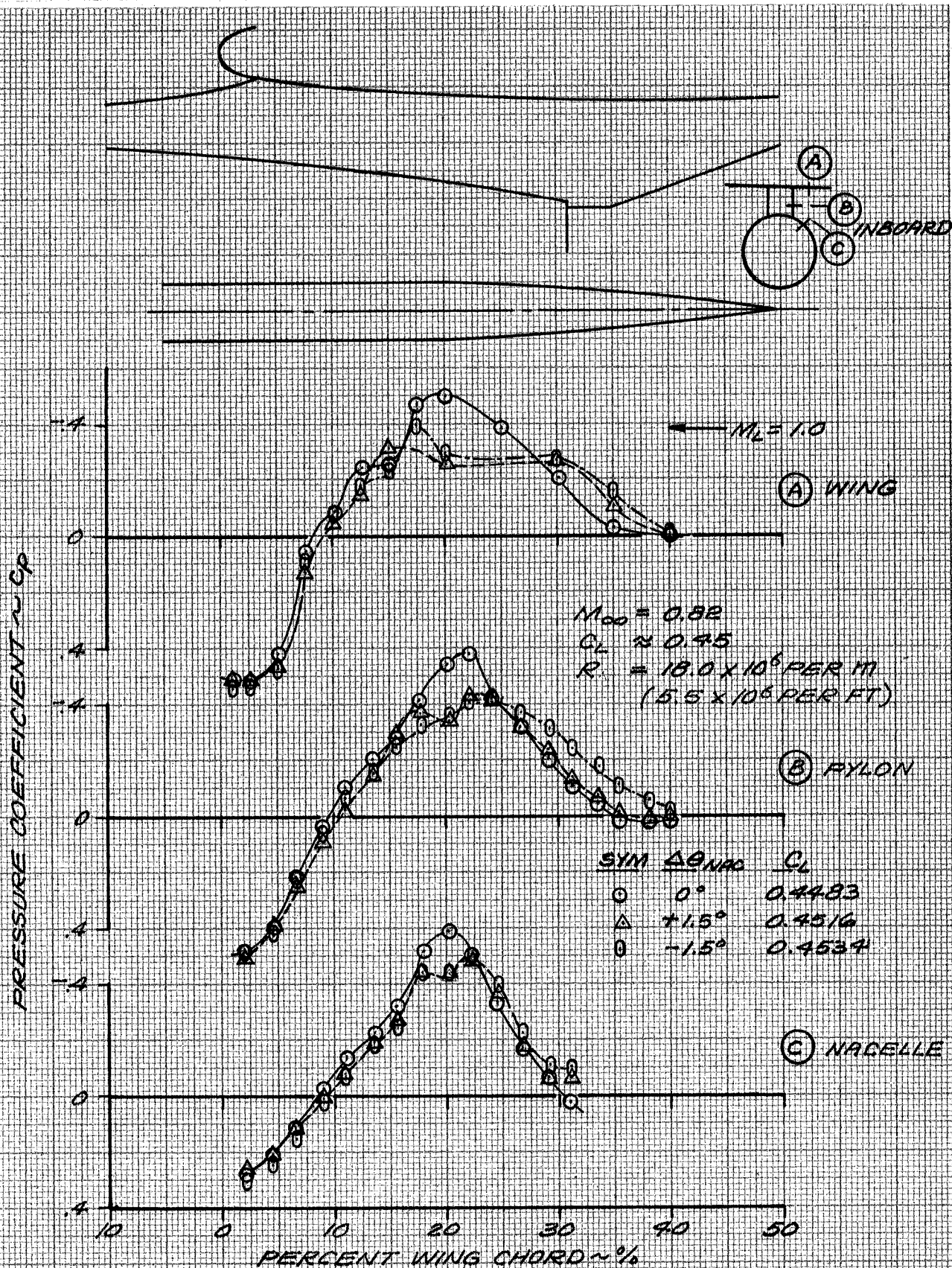(M_∞ = 0.82, C_L = 0.50)

44

FIGURE 26. EFFECT OF NACELLE INCIDENCE ANGLE CHANGE ON INBOARD CHANNEL
PRESSURES — FLOW-THROUGH LDN WITH BASELINE SYMMETRICAL PYLON
(M_∞ = 0.82, C_L = 0.45)

45

entirely due to nacelle-induced drag. Also, the measured incidence penalties are about what would be predicted from isolated nacelle induced drag measurements and previous SDN installed measurements. This further reinforces the conclusion that the channel peak velocities are not high enough to be of concern for the baseline symmetrical pylon.

Pylon Fairings - The effects of the small pylon fairing are shown in Figures 27 and 29 through 32. At C_L = 0.50, the interference drag increments for the small pylon fairing (Figure 27) are about one half those for the baseline symmetrical pylon. The increase in skin friction drags due to the small increase in wetted surface area is insignificant for both pylon fairings. The negative drag increments at 0.6 Mach number at the lower lift coefficients are in all probability not real and are within the capability of the system to measure small drag increments. The channel pressure distributions (Figures 29 through 32) show that the peak pressure coefficients are reduced by about ΔC_p = 0.10 (ΔM = 0.05) across the channel relative to the symmetrical pylon. The pressure gradients aft of the pressure peaks are reduced appreciably on the wing and pylon, and slightly on the nacelle afterbody.

The effects of the larger pylon fairing are shown in Figures 28 through 32. The force data (Figure 28) show a higher interference drag level at 0.6 Mach number. The interference drag level at 0.82 Mach number is about the same as the baseline symmetrical pylon, i.e., not as good as the small pylon fairing. The peak suction pressures in the channel are reduced only slightly relative to the small pylon fairing. The effects of the large pylon fairing are slightly poorer relative to both the baseline symmetrical pylon and the small pylon fairing. In examining the reason for the excess drag of the large pylon fairing, it appears from the channel pressures to be due to a lack of recovery on the nacelle afterbody, and possibly even the result of a local flow separation. Figures 29 through 32 show that the pylon trailing edge recovery is nearly the same for all of the pylons, but there seems to be a distinct effect of the large pylon fairing on the nacelle afterbody recovery near the trailing edge. This is also apparent at 0.6 Mach number. Certainly the large fairing was an over-correction, and a pylon fairing different from either of those tested might offer improved performance.
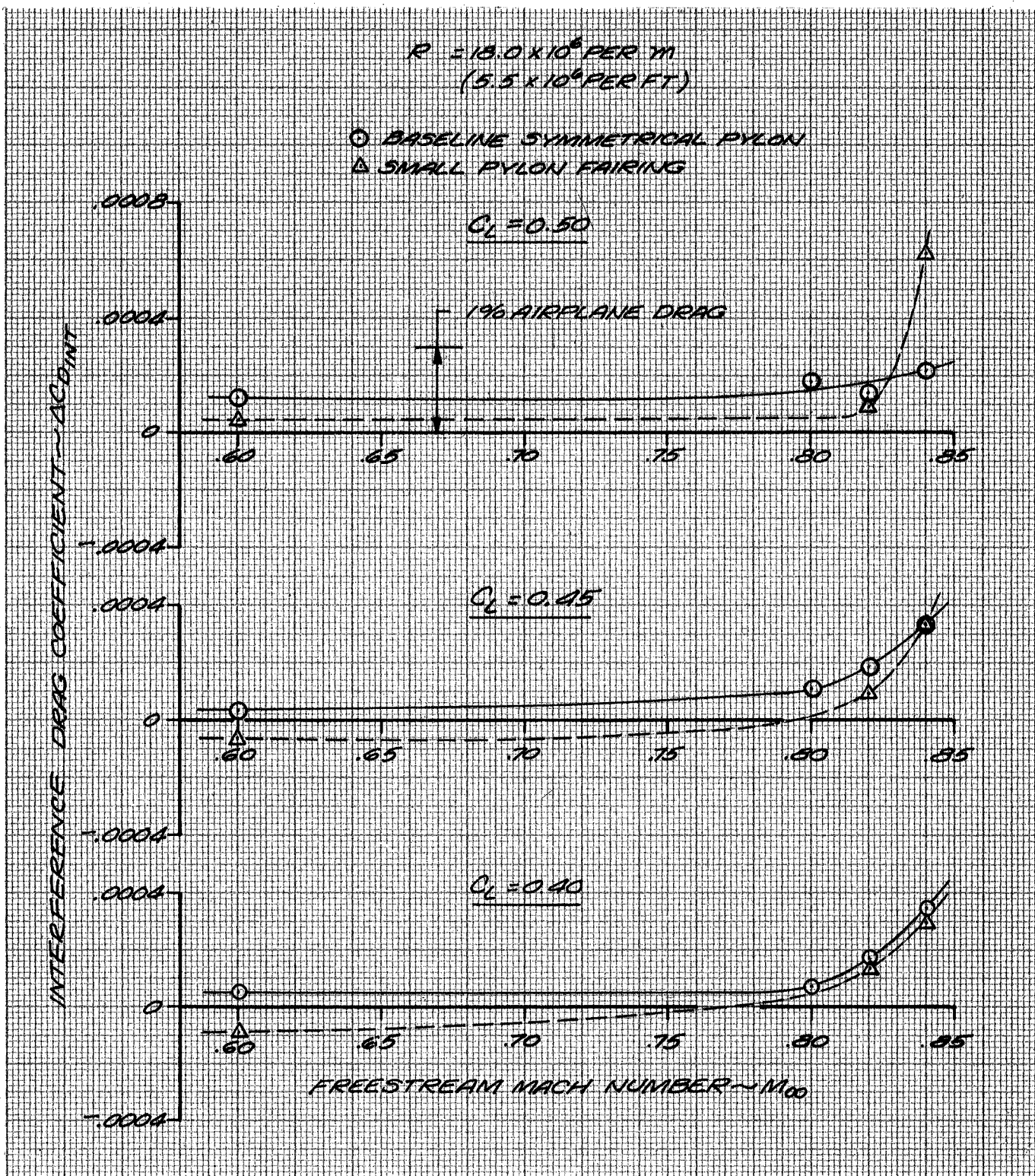
46

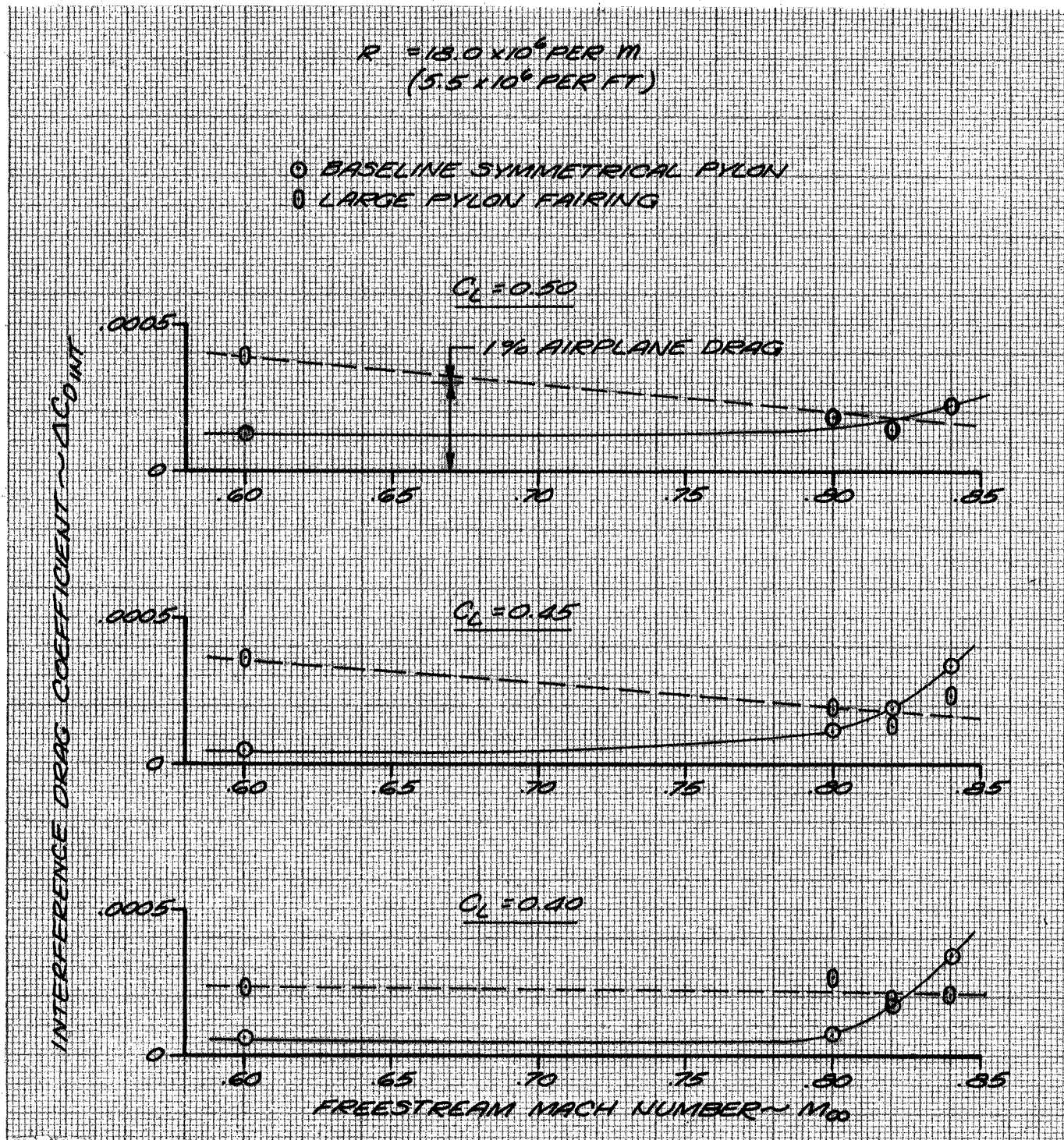FIGURE 27. EFFECT OF SMALL PYLON FAIRING ON LDN INTERFERENCE DRAG

47

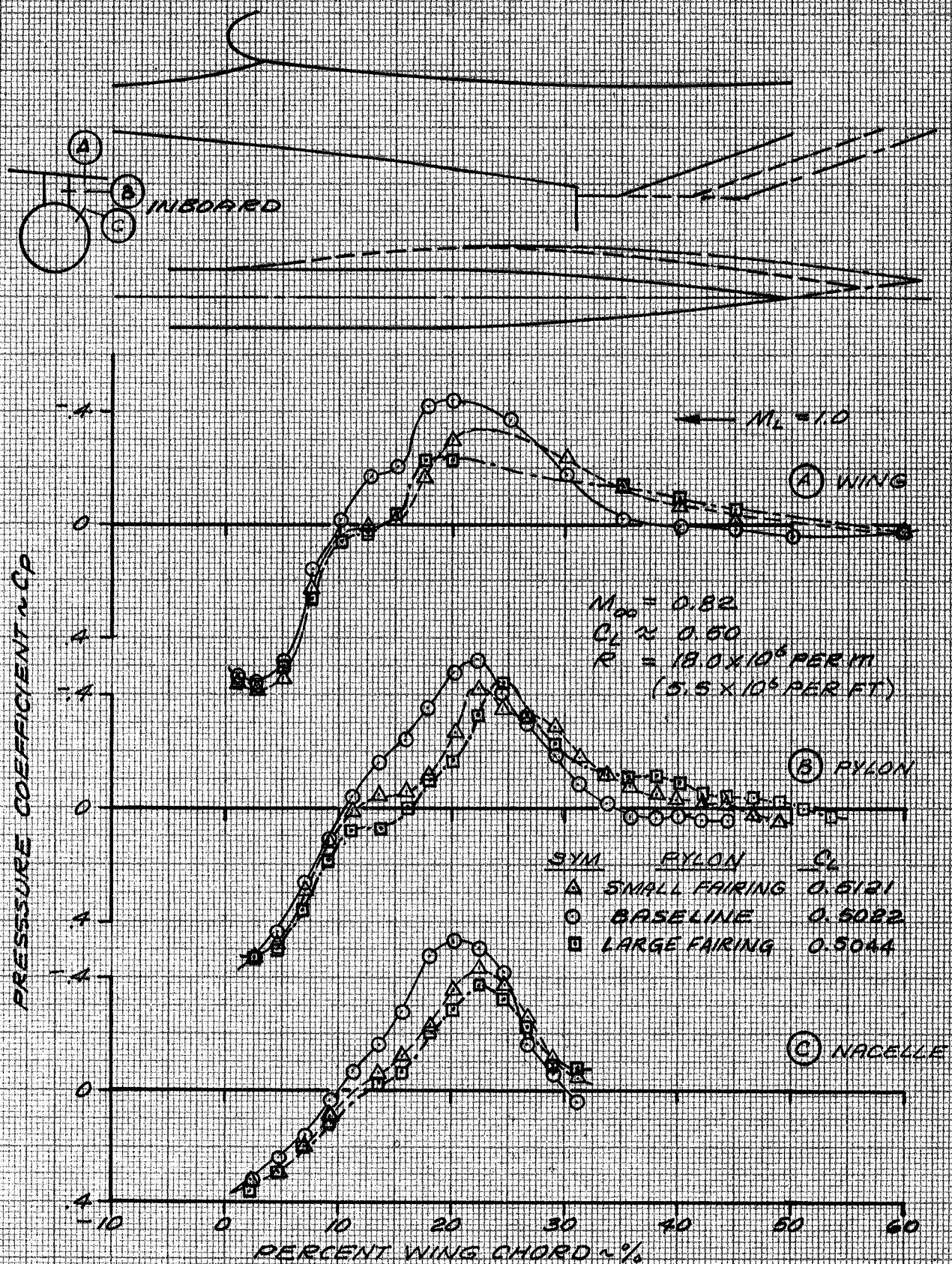**FIGURE 28.** EFFECT OF LARGE PYLON FAIRING ON LDN INTERFERENCE DRAG

FIGURE 29. EFFECT OF PYLON FAIRINGS ON LDN INBOARD CHANNEL PRESSURES
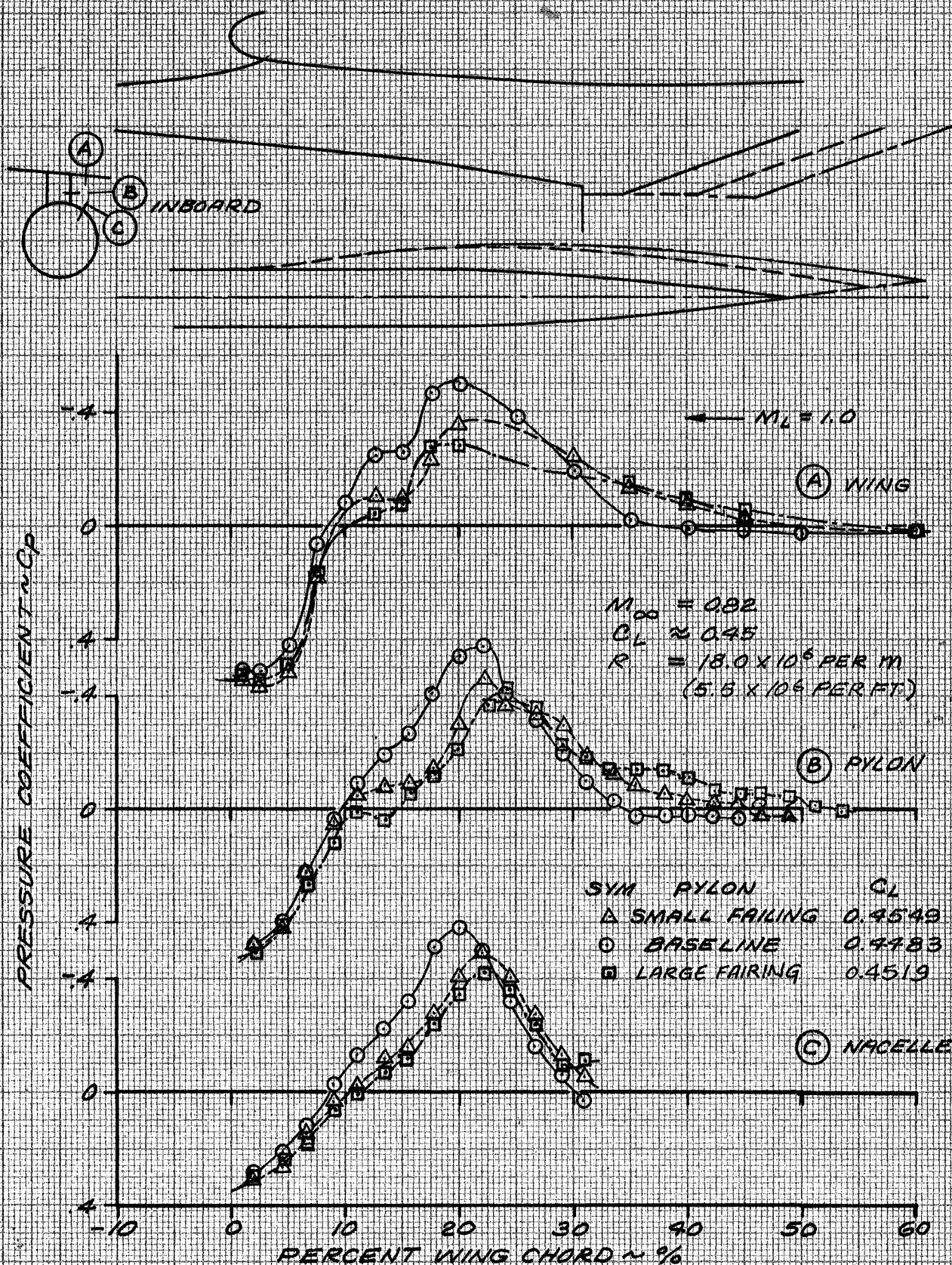$(M_\infty = 0.82, C_L = 0.50)$

$\alpha = 3.2°$

FIGURE 30. EFFECT OF PYLON FAIRINGS ON LDN INBOARD CHANNEL PRESSURES
(M$_\infty$ = 0.82, C$_L$ = 0.45)
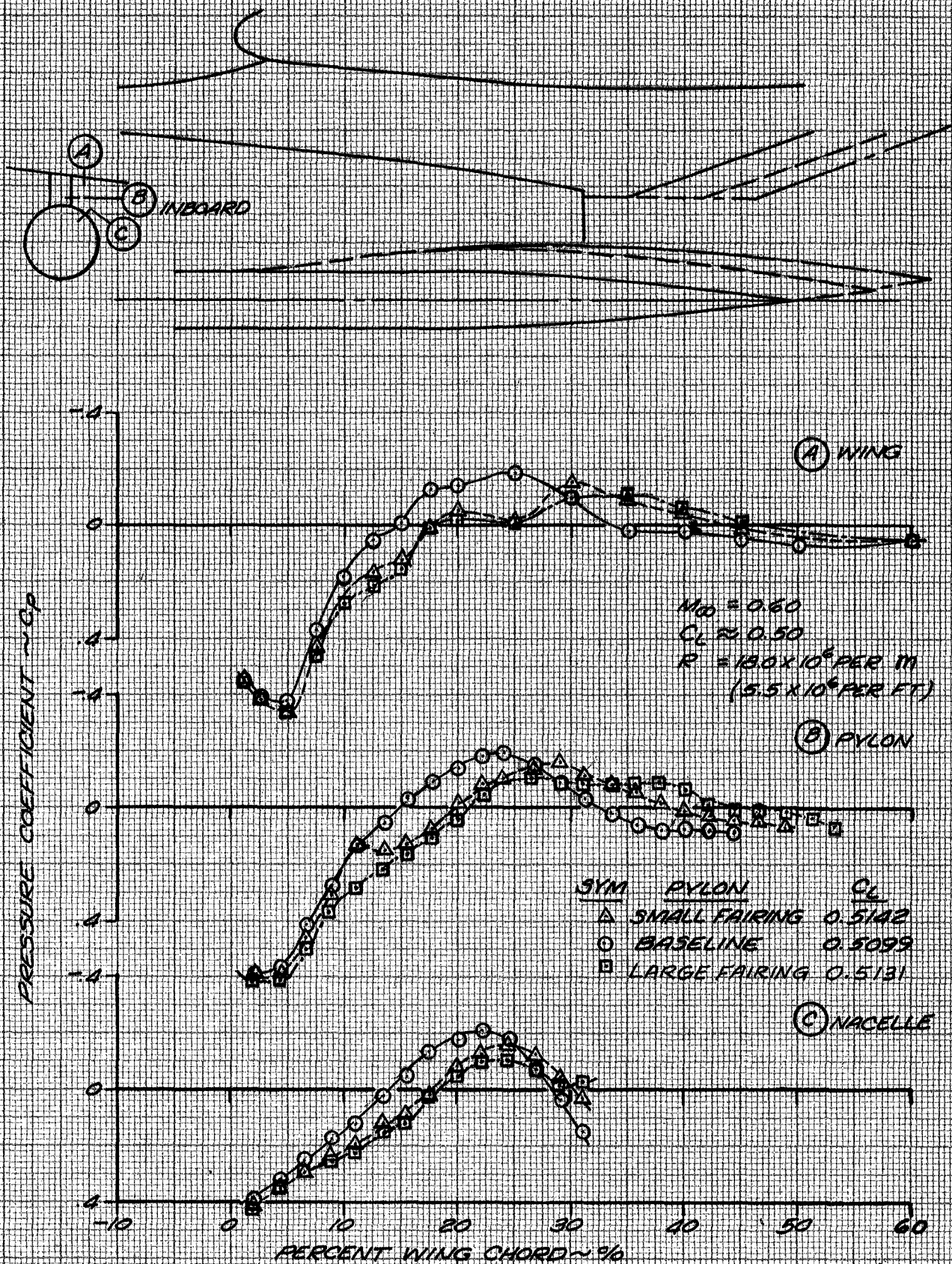
$\alpha = 2.7°$ 50

FIGURE 31. EFFECT OF PYLON FAIRINGS ON LDN INBOARD CHANNEL PRESSURES
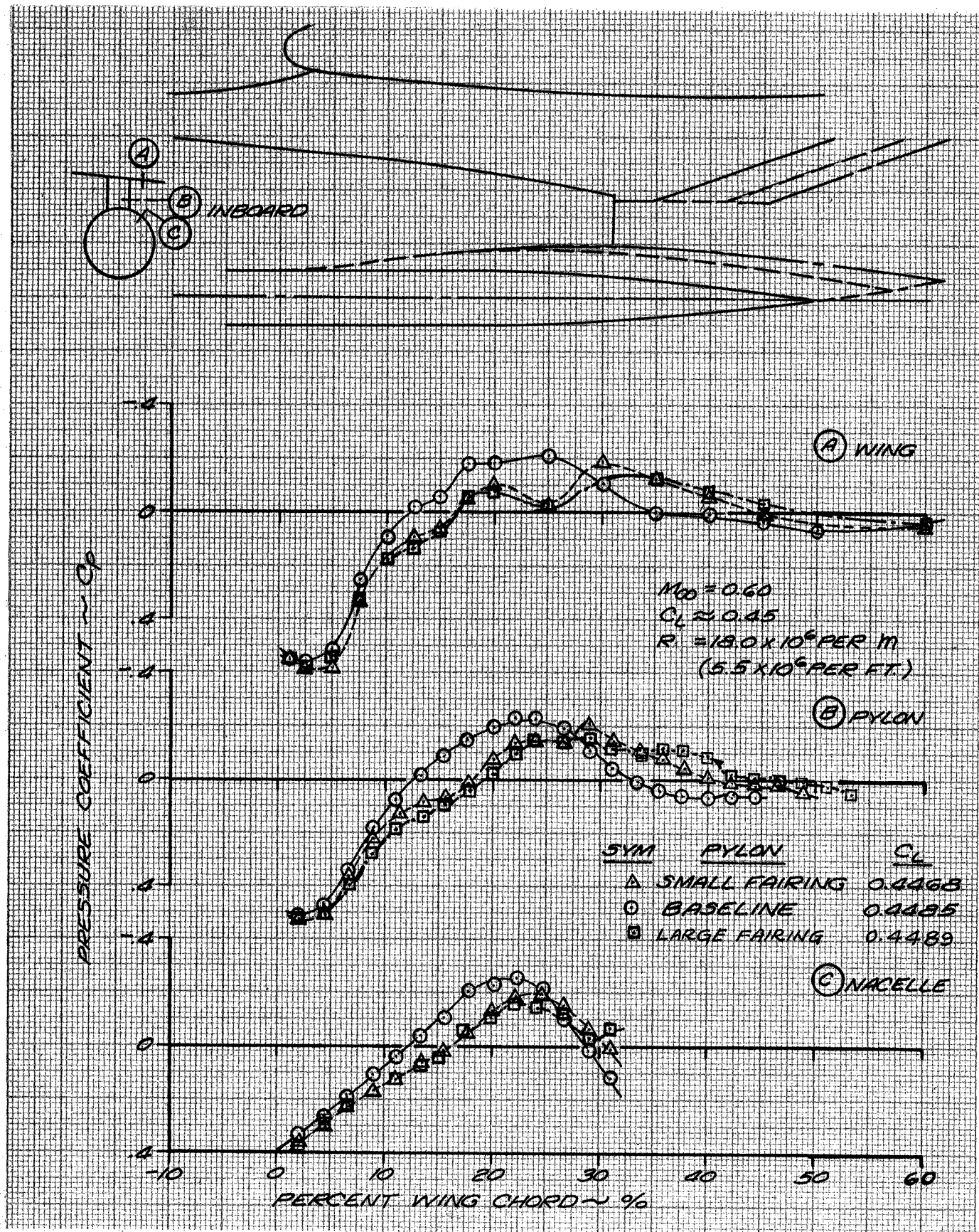$(M_\infty = 0.60, C_L = 0.50)$

FIGURE 32. EFFECT OF PYLON FAIRINGS ON LDN INBOARD CHANNEL PRESSURES
$(M_\infty = 0.60, C_L = 0.45)$

52

Comparison of wind-tunnel measured and the analytically predicted incremental peak-suction-pressure reductions in the inboard channel is shown in Figure 33. The measured reductions in peak pressure coefficient are in reasonably good agreement with those analytically predicted using the potential flow computer code. However, while the absolute peak pressure coefficients are about as predicted at $M_\infty = 0.6$, they are significantly higher at $M_\infty = 0.82$ (refer to Figure 2).
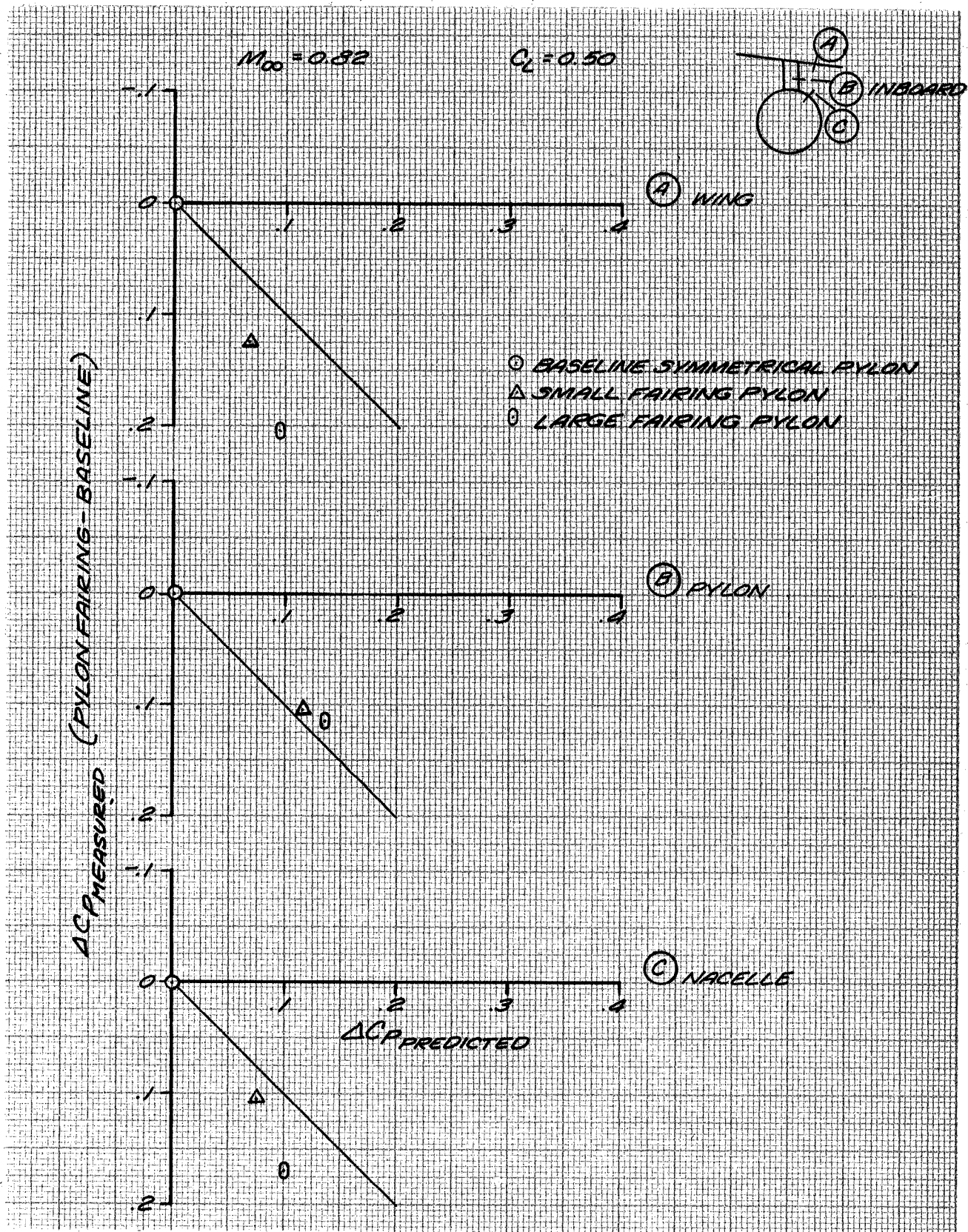
FIGURE 33. COMPARISON OF MEASURED AND PREDICTED CHANNEL INCREMENTAL SUCTION PEAKS FOR PYLON FAIRINGS ($M_\infty = 0.82$, $C_L = 0.50$)

54

CONCLUSIONS

A wind tunnel test to develop a low-drag long-duct nacelle installation applicable to the DC-10 jet transport has been conducted in the NASA Ames Research Center 11-foot transonic wind tunnel. Significant results from this test indicate the following:

1. The long-duct nacelle installation utilizing the current production symmetrical pylon is a low-risk installation for the DC-10 aircraft.

   a. Interference drag penalties of 0.5 percent airplane drag or less are indicated relative to an interference-free installation.

   b. While channel velocities grow with increasing Mach number, the peak values at cruise conditions are significantly less than the values that are known to cause shock-induced flow separations on the nacelle afterbody.

   c. Flow visualization and boundary layer analysis of the pressure data show the flow to be attached on the nacelle afterbody.

2. A small pylon fairing provided an effective means of suppressing the peak channel pressures which resulted in reducing the interference drag penalty to an insignificant level. A larger fairing was not as effective.

3. The incidence angle of the current short-duct nacelle resulted in the minimum drag configuration for the long-duct nacelle.

4. Wing-pylon-nacelle channel pressure distributions obtained with powered simulation or flow-through nacelles were essentially unchanged. This indicates the channel flow was not affected by increasing the exhaust pressure ratio, hence power effects are considered to be negligible.

One of the objectives of this program was to identify the interference drag differences between the long-duct nacelle and the short-duct nacelle. Unfortunately, because of simulator instrumentation problems, this objective was not accomplished. However, the lack of powered force data does not

invalidate any of the conclusions drawn above. On the basis of these results and considerable past experience, the specific LDN investigated would not be expected to significantly change the power-on interference drag relative to the current production SDN installation.

REFERENCES

1. Nordstrom, K. E., Marsh, A. H., and Sargisson, D. F., "Conceptual Design Study of Advanced Acoustic-Composite Nacelles," NASA CR-132703, July 1975.

2. Kutney, J.T., and Piszkin, S. P., "Reduction of Drag Rise on the Convair 990 Airplane," AIAA Preprint No. 63-276, June 1963.

3. Friedman, D. M., "A Three-Dimensional Lifting Potential Flow Program," Volumes I and II, MDC J6182/01 and J6182/02, September 1974.

4. Manual for Users of the Unitary Plan Wind Tunnel Facilities of the National Advisory Committee for Aeronautics, Washington, 1956.

5. Braslow, Albert L. and Knox, Eugene C., "Simplified Method for Determination of Critical Height of Distributed Roughness Particles for Boundary-Layer Transition at Mach Number from 0 to 5," NACA TN 4363, 1958.

6. Cebeci, T., Kaups, K., Ramsey, J. and Schimke, S., "A Two-Point Finite-Difference Boundary-Layer Method for Incompressible and Compressible Two-Dimensional and Axisymmetric Laminar and Turbulent Flows Including Infinite-Swept Wings," MDC Report No. J7986, September 1968.